Journal of Volcanology and Geothermal Research xxx (2018) xxx–xxx

Contents lists available at ScienceDirect

Journal of Volcanology and Geothermal Research

journal homepage: www.elsevier.com/locate/jvolgeores

Growth process of the lava dome/flow complex at Sinabung Volcano during 2013–2016

Setsuya Nakada [a,*], Akhmad Zaennudin [b], Mitsuhiro Yoshimoto [c], Fukashi Maeno [a], Yuki Suzuki [d], Natsumi Hokanishi [a], Hisashi Sasaki [e], Masato Iguchi [f], Takahiro Ohkura [g], Hendra Gunawan [b], Hetty Triastuty [b]

[a] Earthquake Research Institute, The University of Tokyo, 1-1-1 Yayoi, Bunkyo-ku, Tokyo 113-0032, Japan
[b] Center for Volcanology and Geological Hazard Mitigation, Geological Agency, Indonesia, Jalan Diponegoro No. 57, Bandung 40122, Indonesia.
[c] Mount Fuji Research Institute, Yamanashi Prefectural Government, 5597-1 Kenmarubi, Kamiyoshida, Fujiyoshida, Yamanashi 403-0005, Japan
[d] Faculty of Education and Integrated Arts and Sciences, Waseda University, 1-6-1 Nishi-waseda, Shinjuku-ku, Tokyo 169-8050, Japan
[e] Asia Air Survey Co. Ltd., Shinyuri 21 Build., 1-2-2 Manpukuji, Asao-ku, Kawasaki 215-0004, Japan
[f] Sakurajima Volcano Research Center, Disaster Prevention Research Institute, Kyoto University, 1722-19 Sakurajima-Yokoyama, Kagoshima 891-1419, Japan
[g] Aso Volcanological Laboratory, Institute for Geothermal Science, Graduate School of Science, Kyoto University, 3028 Sakanashi, Ichinomiya, Aso 869-2611, Japan

ARTICLE INFO

Article history:
Received 1 August 2016
Received in revised form 29 May 2017
Accepted 15 June 2017
Available online xxxx

Keywords:
Andesite lava dome/flow
Pyroclastic density current
Discharge rate
Cyclic vulcanian events

ABSTRACT

Mount Sinabung, North Sumatra, Indonesia, erupted for the first time in 2010 and reactivated again in 2013. The eruption started with a phreatic phase, changed to phreatomagmatic, and then andesite lava appeared at the summit crater in late December 2013. Lava effusion continued and has been associated with partial to complete collapses of the lava complex, which successively generated pyroclastic density currents (PDCs). The lava complex grew first as a lava dome and then developed into a lava flow (lava extension stage). It extended up to about 3 km in horizontal runout distance by late 2014. When the front of the lava complex moved onto the middle and lower slope of the volcano, PDC events were initially replaced by simple rock falls. Inflation of the upper part of the lava complex began in mid-2014 when the movement of the lava flow front stagnated. The inflation was associated with hybrid seismic events and frequent partial collapses of the upper part of the lava complex, generating PDC events with long travel distances. From mid-September 2014, new lobes repeatedly appeared near the summit and collapsed. Cyclic vulcanian events began in August 2015 when hybrid events peaked, and continued >1.5 years (vulcanian stage). These events sometimes triggered PDCs, whose deposits contained vesiculated lava fragments. The distribution of PDC deposits, which extended over time, mostly overlapped in areal extent with that of the 9th–10th century eruption. Eruption volumes were estimated based on measurements with a laser distance meter during 6 periods, digital surface model (DSM) analysis of satellite images during one period, and the cumulative number of seismically detected PDC events, assuming a constant volume of each PDC event. The total volume of eruption products reached about 0.16 km^3 DRE as of the end of 2015. The lava discharge rate was largest during the initial stage (>7 m^3/s) and decreased exponentially over time. The discharge rate during the vulcanian stage was ≪1 m^3/s. The trend of decreasing discharge rate is in harmony with that of ground deflation recorded by a GPS measurement. The chemical composition of lava slightly evolved with time. Cyclic vulcanian events may have been triggered by limited degassing conditions in the upper conduit and by unloading of the conduit by lava dome collapses.

1. Introduction

Growth of a lava dome and production of a lava flow are common styles of effusive eruption, which can occur before and after explosive events such as plinian or sub-plinian eruptions (Ogburn et al., 2015). Commonly, in lava dome/flow eruptions, the magma discharge and effusion rates are much smaller than in explosive events, and can continue at a low rate for long durations (Pallister et al., 2013). Except for small lava dome/flow eruptions preceded or followed by large explosive eruptions, the final eruptive volumes from lava dome/flow eruptions can be comparable to those of explosive eruptions (e.g., Kozono et al., 2013). Furthermore, collapse of lava from dome/flow margins can generate pyroclastic density currents (PDCs). Therefore, long-lasting lava dome/flow eruptions produce long-term hazards (months to tens of years) from PDCs to residences around the volcano, in contrast to the heavy but short duration impacts of large explosive eruptions. Such long-lasting lava dome/flow eruptions are well documented at the lava dome/flow eruptions at Unzen and Soufrière Hills volcanoes (Nakada et al., 1999; Kokelaar, 2002). In general, PDC generation is

* Corresponding author.
E-mail address: nakada@eri.u-tokyo.ac.jp (S. Nakada).

http://dx.doi.org/10.1016/j.jvolgeores.2017.06.012

not limited to the early stage of eruptions when discharge rate is high. Large PDCs from dome/flow failure may also become frequent in the late stage of eruption due to high potential energy as the dome complex grows and steepens. As the mode of lava dome/flow growth is not simple, understanding its diversity and controlling mechanism is important to minimize risks from all hazards related to lava dome/flow eruptions, not just PDC events. For example, sudden explosive events are common during lava dome/flow growth (e.g., Nakada et al., 1999; Druitt et al., 2002; Bluth and Rose, 2004). The mechanisms of changing from effusive to explosive modes have been discussed by several researchers (e.g., Melnik and Sparks, 1999; Holland et al., 2011; Boudon et al., 2015). The Sinabung lava dome/flow-forming eruption, which continues even when this manuscript was being written, is a new example of a long-lasting lava dome eruption, similar to those at Unzen and Soufrière Hills. However, Sinabung entered into an explosive stage at a time when growth of the lava dome/flow had almost stopped. This eruption gives us an excellent opportunity to learn new aspects of lava dome/flow eruptions. Although it shows similar aspects to previous lava dome-forming eruptions such as Mount St. Helens during 1980–1986, Unzen volcano during 1991–1995, and Soufrière Hills volcano from 1995 (Swanson and Holcomb, 1990; Nakada et al., 1999; Kokelaar, 2002), several points, such as the long extension of a single lava flow, successive inflation of this lava flow, and cyclic explosive events in the later stage, are clearly different from these other examples. In this paper, we describe the growth process of the lava dome/flow at Sinabung and its associated eruption phenomena, and we discuss the mechanisms of lava dome/flow growth and the change of eruption mode. For clarity, the lava dome/flow complex formed in this eruption is called the lava complex.

2. Background of Sinabung Volcano

Sinabung Volcano, in Karo Prefecture, North Sumatra, Indonesia (Fig. 1), is an example of a volcano without a historic record of eruption. It was activated with a phreatic eruption in August–September 2010 (Global Volcanism Program, 2010; Sutawidjaja et al., 2013). Resumption of eruptive activity subsequently occurred in September 2013 (Global Volcanism Program, 2013, 2014a, 2014b). In December 2013, activity shifted to a lava dome/flow-forming eruption and continued for more than three years.

A joint Indonesian-Japanese research team started a geological study of Sinabung Volcano soon after the eruption in 2010 (Iguchi et al., 2012; Prambada et al., 2011). Sinabung is a stratovolcano built above the ignimbrite plateau of the Toba caldera super eruption of approximately 73 ka before present (Chesner et al., 1991). The summit of Sinabung is approximately 2460 m above sea level (asl) and the base of the volcano lies at approx. 1000 m asl (Fig. 2). The last magmatic pre-historical eruption occurred in the 9th–10th century (Iguchi et al., 2012). The present eruption is similar to this previous eruption in terms of the eruption type, distribution of products, and lava composition.

The basement rocks of the volcano are exposed northwest of the edifice and the older edifice of this volcano is exposed mainly in the west, whereas the younger edifice occupies the central and eastern areas (Iguchi et al., 2012). Deposits within the edifice consist mainly of lava flows/domes and PDC and debris-flow deposits. The younger edifice shows no pumice-fall deposits indicative of plinian-type eruptions. Several pre-historic lava flows extend from the summit down to the lower slopes of the volcano, and relatively thick lava flows pile up on the upper slopes, and lava dome/flow collapse-type PDC (block-and-ash flow) deposits are extensively distributed at the volcano's foot. A small-scale debris avalanche deposit is preserved at the northeastern foot of the volcano. The 9th–10th century PDC deposits are widely distributed on the southeastern slope and the associated lava flows extend about 1.5 km from the summit crater. The travel distance of those PDCs is calculated to be about 4.5 km from the summit. Two connected craters each about 150 m across lie on the eastern shoulder of the summit with a NE–SW alignment. Those craters became the site of the lava vents for the current eruption (Fig. 2). A lava spine stands on the southern rim of the southwestern crater, and two small pits opened at the base of this spine, which were formed during the 2010 phreatic events (e.g., Global Volcanism Program, 2010). Strong fumarolic activity occurred from these open pits and on the upper slope of a large gulley extending from the summit to the south, leaving sulfur deposits on the surface that were visible from a distance (Sutawidjaja et al., 2013).

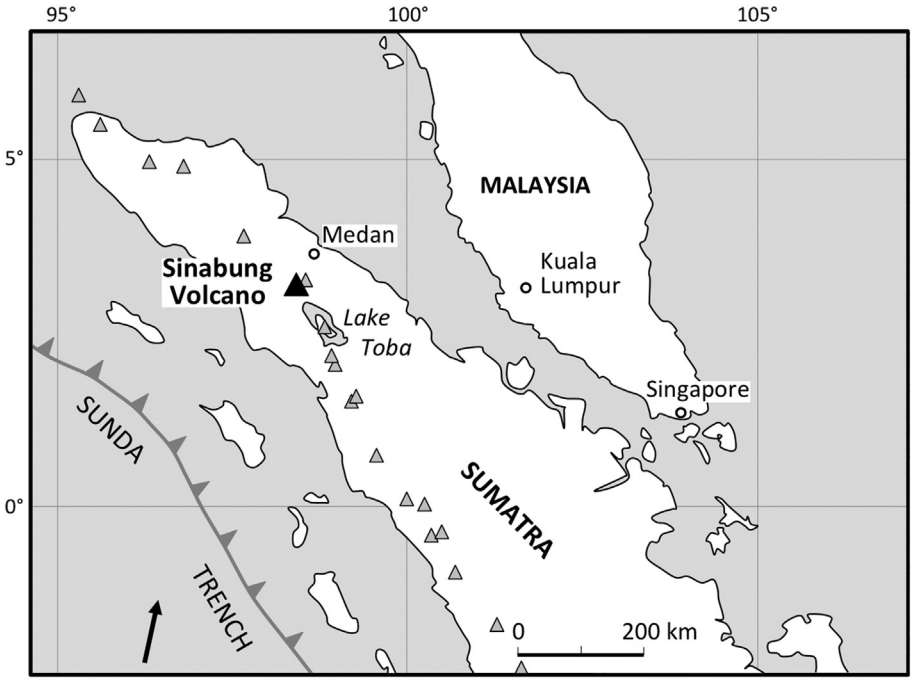

Fig. 1. Index map of Sinabung Volcano. Small gray triangles show other active volcanoes. The arrow showing plate movement direction is after Hill et al. (2012).

Please cite this article as: Nakada, S., et al., Growth process of the lava dome/flow complex at Sinabung Volcano during 2013–2016, J. Volcanol. Geotherm. Res. (2018), http://dx.doi.org/10.1016/j.jvolgeores.2017.06.012

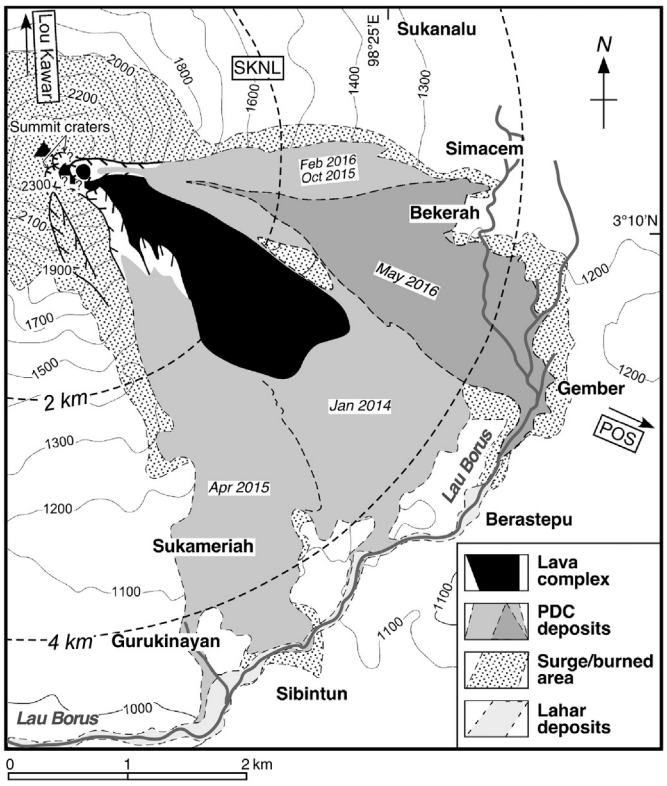

Fig. 2. Distribution map of the lava complex, pyroclastic density current (PDC) deposits, and lahar deposits at Sinabung Volcano. The depositional area for the May 21, 2016 PDC deposits is shown separately. The months and years on the depositional areas represent the main time periods for depositions in these areas. The SPOT 6 image on May 31, 2016 was used to determine the distribution limits of the lava and PDC deposits. Village names are shown in bold font in their approximate localities.

Sinabung volcanic rocks are basaltic andesite to andesite, containing hornblende phenocrysts (Iguchi et al., 2012). The lava spine, which was probably hornblende andesite, although it experienced high levels of hydrothermal alteration and silicification, and resulting in a high-silica composition (Appendix Table 1).

3. Method of topographic measurement

3.1. Laser distance meter

We used a laser distance meter to measure the topographical and volume change of the lava complex. We mapped the surface of the lava complex, its surrounding talus, and non-deformed mountain slopes with a Vectronix Inc. VECTOR 21 binocular dimensional digital compass (laser distance meter). The reference points were set on bare rocks on the mountain slope beside the growing lava complex. We repeatedly shot the laser against both unknown targets and reference points from the Center for Volcanology and Geological Hazard Mitigation (CVGHM) Sinabung Volcano Observatory (POS), measuring the horizontal and vertical distances between the targets, the reference points, and POS. By using positions of the reference points determined from a topographical map that was made before the eruption using ASTER data (30 m spatial resolution; GDEM released on June 29, 2009), the positions of the other targets were geometrically determined relative to the coordinates of POS, which were defined as zero (0,0). The relative error of measurement is around 20 m, considering the accuracies of laser focusing (±5 m at >2 km distance, based on the instrument manual) and the ASTER topographic map. The error of calculated volume estimation of the lava complex is considered to be about 15–10%. The measured dimensions of the lava complex and the volumes for several periods are shown in Fig. 3 and Table 1.

3.2. Digital surface model (DSM)

The commonly cloudy conditions and eruption clouds at Sinabung Volcano made it very difficult to obtain paired satellite images suitable for topographical measurement. We used satellite images from Pleiades data of June 27, 2015 and SPOT-6 data of July 5, 2015 to make a DSM at the end of June 2015. In both of these sets of images, the summit and parts of the eastern slope were covered by an eruption cloud. Topography data from before the eruption were taken from the Shuttle Radar Topography Mission (STS-99 in 2000) (SRTM-1) with a resolution of about 30 m. Fig. 4A shows the 3D image of the end of June 2015 that was produced from those satellite images. We calculated differences in height before and during eruption using the above DSM data, interpolating the original data of 2-m intervals into 30-m spacing to match SRTM-1 data. The height difference model is shown in Fig. 4B. We calculated the volume of eruption products within the area of new lava and pyroclastic deposits (Fig. 2). The relative error of height difference calculation is around 10 m, considering the resolutions of satellite image processing and SRTM-1 data. To calculate the dense-rock equivalent (DRE) volume of pyroclastic deposits, we used a density of 1400 kg/m^3, which was based on in field density measurements. The density of lava was taken here as 2500 kg/m^3, assuming it was non-vesicular.

4. Eruption sequence and lava complex growth

4.1. Lava appearance at the summit

The current eruption of Sinabung, which resumed with a phreatic explosion on September 15, 2013 (Global Volcanism Program, 2013) and increased in intensity over the initial few months, such that the frequency of eruption and the height of eruption plume increased. In mid-November 2013, the eruption style changed into a vulcanian type, which lasted until mid-December when lava extrusion began. The eruption column of the November 18 event reached about 8.5 km above summit (Global Volcanism Program, 2013). Column-collapsed PDCs were observed with the travel distances of about 1 km and 0.5 km, respectively, on November 5 and 19, 2013. Presence of juvenile particles was confirmed first in volcanic ash of November 11, 2013 (manuscript in preparation) and pumice fragments of a few cm across were found in the products of the November 23, 2013 eruption.

Volcanic seismicity increased before the appearance of the first lava at the summit on December 18, 2013 (Gunawan et al., this issue; McCausland et al., this issue). The number of deep-seated volcano-tectonic events increased beginning in July 2013, and shallow volcano-tectonic events increased when the phreatic eruption resumed in mid-September 2013. Low-frequency events started in early December 2013, and soon after hybrid events started. According to a GPS study (Hotta et al., this issue), the baselines between the northern part of the volcano (Lou Kawar) and the Sinabung Volcano Observatory (POS) and between the Sukanal station about 2 km northeast of the summit and the POS slightly lengthened over time, increasing in rate of change just before the appearance of lava (Fig. 5A). Hybrid events increased rapidly in the beginning of December 2013, after summit eruption stopped, peaked just before the appearance of lava, and then continued, reaching a greater event-rate peak in mid-January 2014 (Fig. 5B). This type of seismicity was considered to be associated with magma rising to just beneath the summit crater.

The eastern outer slope (POS side) of the northeast crater at the summit underwent large-magnitude deformation and small slumping of the slope occurred in mid-December 2013 (Pallister et al., this issue). According to Gunawan et al. (this issue) and Pallister et al. (this issue), lava first appeared on December 18 on the eastern rim of the

Please cite this article as: Nakada, S., et al., Growth process of the lava dome/flow complex at Sinabung Volcano during 2013–2016, J. Volcanol. Geotherm. Res. (2018), http://dx.doi.org/10.1016/j.jvolgeores.2017.06.012

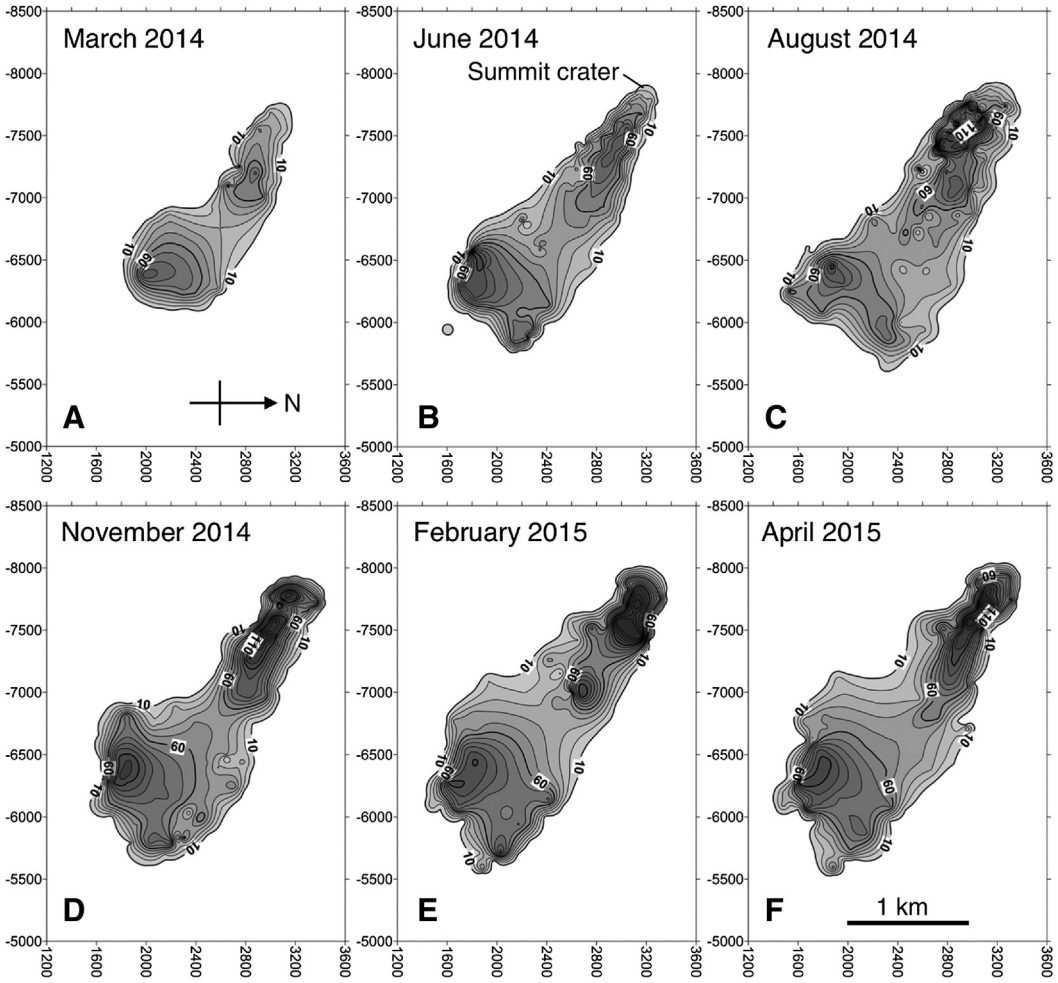

Fig. 3. Isothickness maps of the lava complex for different 6 periods at Sinabung Volcano based on on-site measurement with a laser distance meter. X and Y axes show the horizontal north-south and east-west distances, respectively, setting the coordinates of the Sinbung Volcano Observatory (POS) at the origin (0,0). The figures on the X and Y axes increase toward the north and east, respectively. Thickness contours are drawn at 10 m intervals. The thicker the lava complex is, the darker in color.

northeast crater, which had already been deformed by this time, and lava extrusion produced a lava dome >50 m across by December 20. Rock falls, which could be counted seismically, began on December 20, 2013. The approximate size of the lava dome was about 250 m long and 200 m wide on December 30, 2013.

PDC events caused by partial collapses of the growing lava dome started on December 30, 2013. Eruptions directly from the summit crater were not witnessed during this period. CVGHM recorded most of PDC events as “letusan” (eruption), instead of “awan panas” (PDC). For example, no PDC events were counted by CVGHM during January 12–February 16, including events that we witnessed in the field and that included the February 1, 2014 event that caused 16 fatalities. It seems that soon after PDC producing events began, confusion existed among POS observers in routine distinction between collapse-generated PDC events and vertical-directed eruptions. The number of rock falls counted seismically in the POS was high during this period and increased again around the end of January, when the major PDC event occurred on February 1. Therefore, the daily numbers of eruption events

Table 1
Cumulative volume estimates in millions of m^3 for the lava complex and PDC deposits for different periods at Sinabung Volcano.

Periods	Methods	Lava complex_*a*	Pyroclastic deposits_*a*	Lava complex_*b*	Pyroclastic deposits_*b*	Total (DRE)
2014/3/22	Laser distance meter	32–44	?	31.8	39.0	60.1
2014/6/6	Laser distance meter	59–76	?	58.6	40.1	89.2
2014/8/14	Laser distance meter	73–94	?	73.1	40.5	104.9
2014/11/28	Laser distance meter	89–110	?	87.6	53.9	128.7
2015/2/1	Laser distance meter	92–115	?	91.6	66.5	140.6
2015/4/11	Laser distance meter	93–117	?	93.1	71.5	145.2
2015/6/25	GIS/WroldView-2	108.9	66.8	97.0	77.4	152.9
2015/12/31		?	?	97.0	90.5	161.0

_*a*: Raw volume data which were calculated by using the original laser measurement and DSM data.
_*b*: Calculated volumes by considering pyroclastic (talus) deposits buried under the lava complex.
Densities of lava and pyroclastic deposits for dense-rock equivalent (DRE) were assumed to be 2500 and 1400 kg/m^3, respectively.

Please cite this article as: Nakada, S., et al., Growth process of the lava dome/flow complex at Sinabung Volcano during 2013–2016, J. Volcanol. Geotherm. Res. (2018), http://dx.doi.org/10.1016/j.jvolgeores.2017.06.012

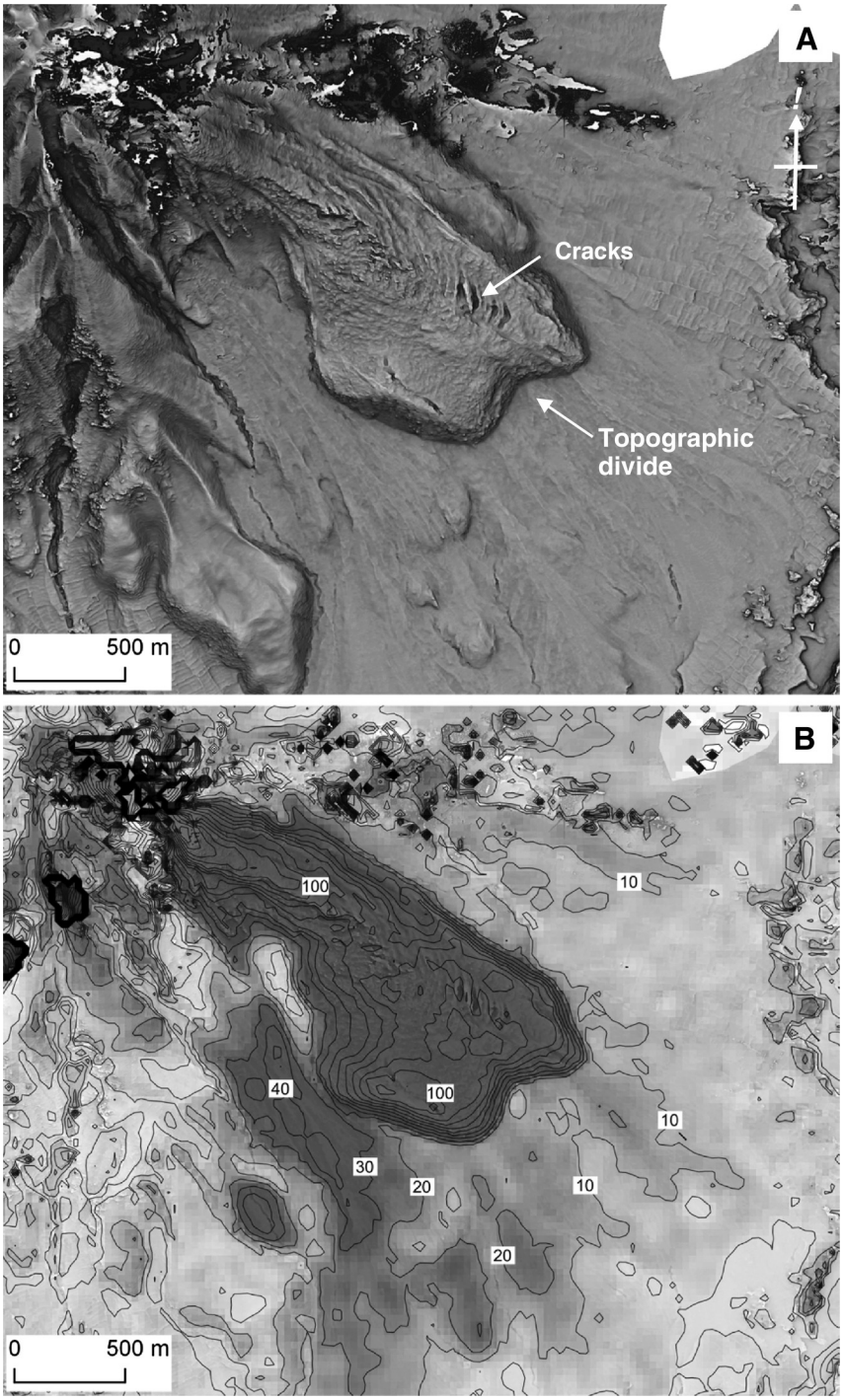

Fig. 4. Relief map of the southeastern part of Sinabung Volcano based on the digital surface models (DSMs) for the Pleiades image on June 27, 2015 and SPOT-6 image on July 5, 2015 (A) and the difference in elevation between the above data and the Shuttle Radar Topographic Mission (SRTM)-1 data taken in 2010 (B). The contour interval is 10 m.

during the above period recorded by CVGHM were changed to those of lava collapse-generated PDC events in this paper (Fig. 5B and C).

4.2. Extension of the lava complex

CVGHM observers in the POS monitored the activity of the lava complex by taking daily photographs. In early January 2014, photographs show that the lava dome was growing to the southeast (the direction of POS), and was dark gray with a rugged surface showing rough convex-downward creases. Until early January 2014, the base of the growing dome was nearly flat and paved with talus deposits consisting of fresh gray boulders and fragments of new lava, and occupying a relatively wide area in the headwater of a small valley. The lava dome imaged by TerraSAR-X on January 18, 2014 was in a cocoon-like form about 420 m long and 160 m wide and occupied the summit crater and extended to the southeast from the original crater rim. This dome was considered to have been extruded after a large collapse on January 5, 2014 (Gunawan et al., this issue; Pallister et al., this issue). Lava moved along the area of lowest topography on the upper slope. By the end of January 2014, the moving front of the lava reached mid-slope, which is shallower than the upper slope (~1.1 km runout from the crater) (Figs. 6A and 7B), and partial collapses occurred frequently in the

Please cite this article as: Nakada, S., et al., Growth process of the lava dome/flow complex at Sinabung Volcano during 2013–2016, J. Volcanol. Geotherm. Res. (2018), http://dx.doi.org/10.1016/j.jvolgeores.2017.06.012

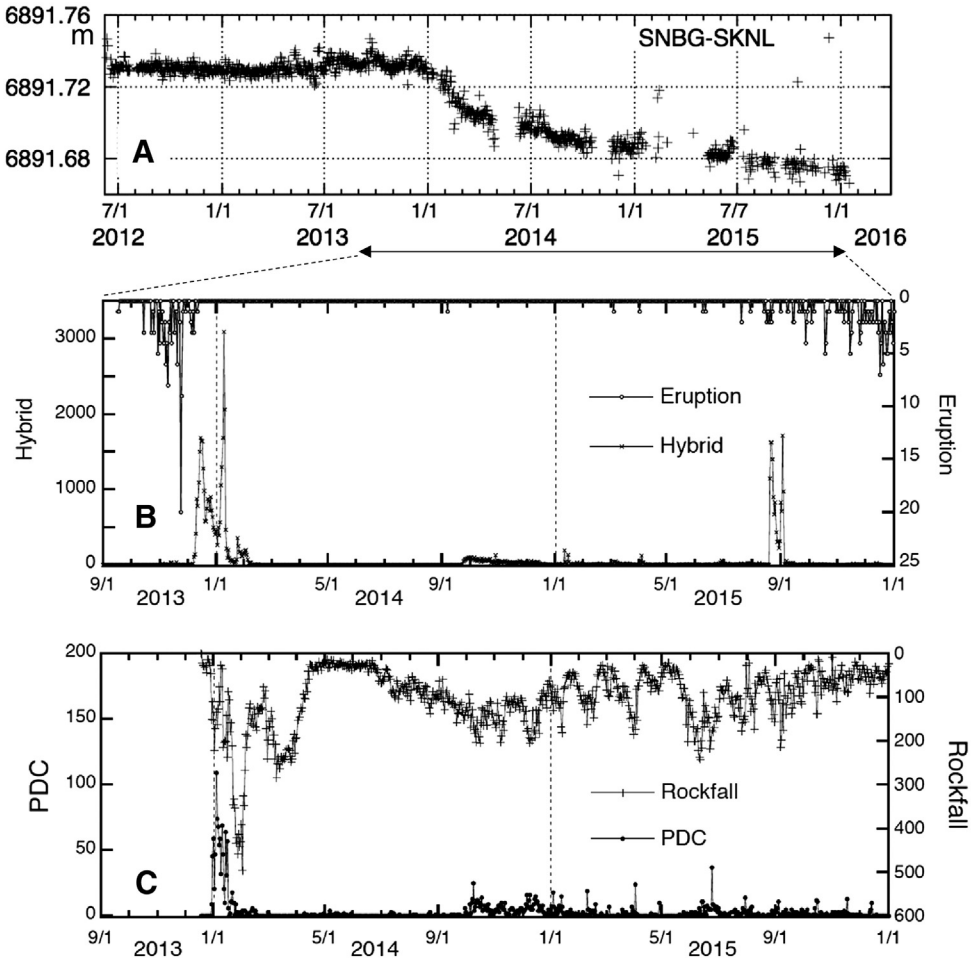

Fig. 5. Temporal changes in a GPS baseline length, and daily numbers of seismically determined hybrid, eruption, pyroclastic density current (PDC), and rock fall events at Sinabung Volcano. A: The baseline length between Sukanalu (SKNL in Fig. 2) and the volcano observatory (POS) in m, is modified from Hotta et al. (this issue). B: PDC event and eruption from CVGHM. C: PDC events and hybrid events from CVGHM. The boundary between lava extension and inflation stages is marked by a weak increase of hybrid events and increasing PDC events in mid-September 2014, while that between inflation and vulcanian stages is marked by strong peaks in August 2015. In C, the number of PDC events during January and February 2014 was modified from the original data (see the text for detail).

moving front. Small collapses also occurred in the upper-slope area and resultant PDCs descended along both margins of the lava complex (Fig. 7B). Partial collapses that generated PDC events were dominant in the first one month when the lava was moving down the upper slope, and then rock falls became dominant instead, when the lava moved to the middle slope (Fig. 5C). Furthermore, rock falls hardly occurred at all when the moving front reached the volcano foot in March 2014. The moving front reduced in speed and almost stopped at the end of 2014 (Figs. 7A and 7C). Then, around June 2014, the lava complex moved over a small topographic divide at the foot. As this divide behaved as an obstacle for the moving lava, the northeastern part of the lava complex, which was moving in a lower elevation, advanced forward and expanded northward, away from the central and southwestern parts (Fig. 7A). As this northeastern part continued moving until November 2014, crevasse-like cracks developed along a shear zone between the moving northeastern part and the remaining central to southwestern part. The place with the thinnest pyroclastic deposits, just in front of the middle frontal cliff of the lava complex (Figs. 2 and 4A) is the location of the divide. Infrared camera views (Fig. 8) show highest temperature areas limited to the moving marginal brittle parts of the lava complex, suggesting repetition of partial collapses at the margins rather than the central parts of the lava complex. Preferential movement of the northeastern frontal part of the flow in June 2014 (right side in Fig. 8B) contrasts to homogenous movement of the lava front in March 2014 (Fig. 8A). The advance speed of the lava flow was >60 m/d when it was on the upper slope during the first two months, about 20 m/d on the middle slope during the following few months, and down to 2 m/d at the foot during the period after mid-2014 (Fig. 7C).

4.3. Inflation of the lava complex

According to CVGHM seismic data, low frequency (LF) events that had stopped in the earliest stage of lava dome growth, restarted in early September 2014, and hybrid events increased in late September 2014 (Fig. 5B). The outline of the lava complex had hardly changed after November 2014 (Figs. 3D–F and 7A). However, the maximum elevation of the upper part of the lava complex increased over time (Fig. 7D) until mid-2015, even after the elongation of the lava complex had almost stopped in mid-2014. This fact implies that the lava complex, especially in and around the upper part, thickened continuously until mid-2015 (Fig. 3B–D).

As the surface of lava stopped growing it turned lighter and brown in color over time, meaning that the new growing mound (lobe) could be identified by its grayish color (Fig. 6D). New lobes repeatedly appeared in the southern side of the upper part of the lava complex since mid-September 2014 (Gunawan et al., this issue), when the numbers of hybrid and PDC events increased (Figs. 5B and C). The new lobe was like a bud of dark gray lava at first, about 30–50 m across, and then grew large

Please cite this article as: Nakada, S., et al., Growth process of the lava dome/flow complex at Sinabung Volcano during 2013–2016, J. Volcanol. Geotherm. Res. (2018), http://dx.doi.org/10.1016/j.jvolgeores.2017.06.012

Fig. 6. Representative photographs of the growing lava complex and eruptive events at Sinabung Volcano. A: Incandescence of growing lava flow on the southeastern slope taken at the Bamboo site (6.5 km ENE of the summit) on the early morning of January 25, 2014. B: Lava complex, the front of which had reached the lower slope on March 22, 2014. C: Lava complex at close to maximum advance on June 6, 2014. D: New lava lobe (a black mound with dust clouds in center-left) growing on the south side of the top of the lava complex (extending from the center to the bottom), the latter of which became knife-edge-shaped in the uppermost part due to erosion by repeating partial collapses on both sides. Photo taken near Gember (5 km ESE of the summit) on February 3, 2015. E: Pyroclastic density current (PDC) event on February 1, 2014, taken from POS. F: A vulcanian event that simultaneously triggered a partial collapse of the upper lava complex, which descended as PDCs on September 15, 2015. G: An event generating PDCs to both sides of the lava complex on October 31, 2015. H: Deposits of PDC event on May 21, 2016. Photographs except for A and D were taken by the Indonesian Center for Volcanology and Geologic Hazard Mitigation (CVGHM) observers, about 9 km east-southeast of the summit.

like a cocoon, about 200 m long, 100 m wide, and 50 m high in late October 2014. There were repeated partial collapses from its moving front and sides (Fig. 6D). Each new lobe disappeared due to multiple partial collapses after reaching a length of about 200 m in 2015 and shorter in 2016. After major lava collapse events, new lobes reappeared in the same location. Throughout 2015, similar growth and collapse cycles were repeated in roughly one-month intervals. Large PDC events were always associated with multiple smaller events, thus high PDC event numbers were repeated, appearing as monthly spikes after the second half of 2014 in Fig. 5C.

In June 2015, a new lava lobe appeared in the northeastern side of the upper part of the lava complex and PDCs started descending to the east (Fig. 2). On April 11, 2015, the lobe on the southwestern side was about 160 m long, 140 m wide, and 50 m high, with an approximate volume of 5.6×10^5 m^3. It was emplaced within 8 days after a large collapse on April 2, 2015, giving an effusion rate of about 0.7 m^3/s over that week.

Please cite this article as: Nakada, S., et al., Growth process of the lava dome/flow complex at Sinabung Volcano during 2013–2016, J. Volcanol. Geotherm. Res. (2018), http://dx.doi.org/10.1016/j.jvolgeores.2017.06.012

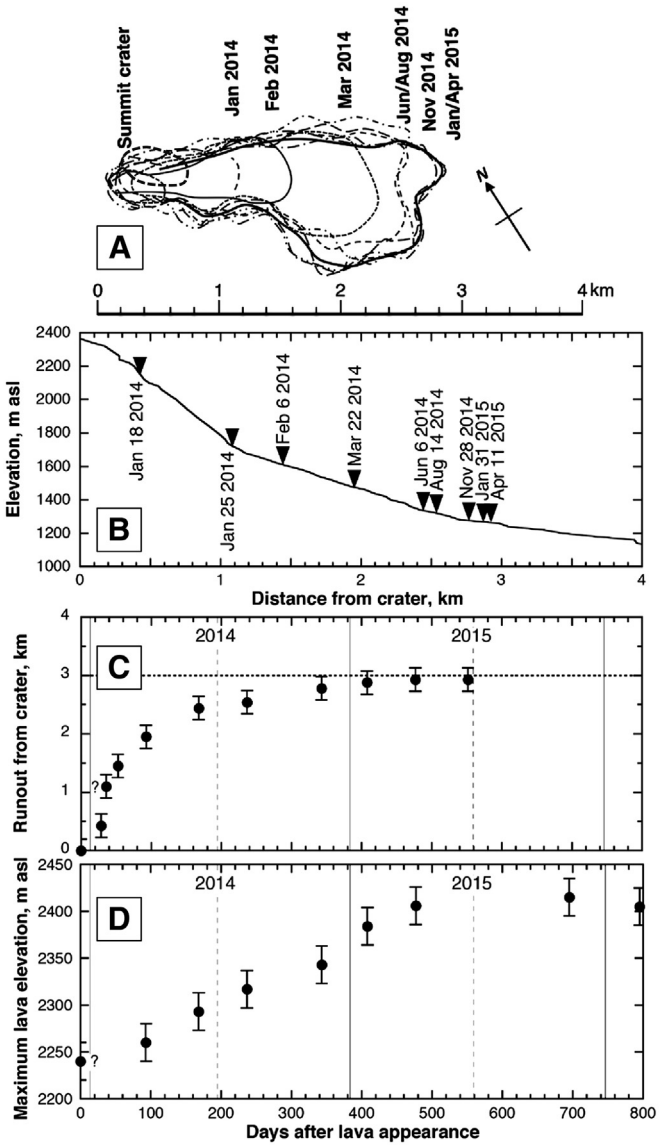

Fig. 7. A: Growth pattern of the lava complex at Sinabung Volcano. B: The original topographic section along the elongation of the lava complex. C: The temporal change of the lava complex elongation. D: The temporal change in maximum elevation of the upper part of the lava complex. The outlines of the lava complex for several periods were based on our measurements with a laser distance-meter, and taken from January 18, 2014 TerraSAR-X image, and NASA from February 12, 2014, and DSM at the end of 2015 (Fig. 4).

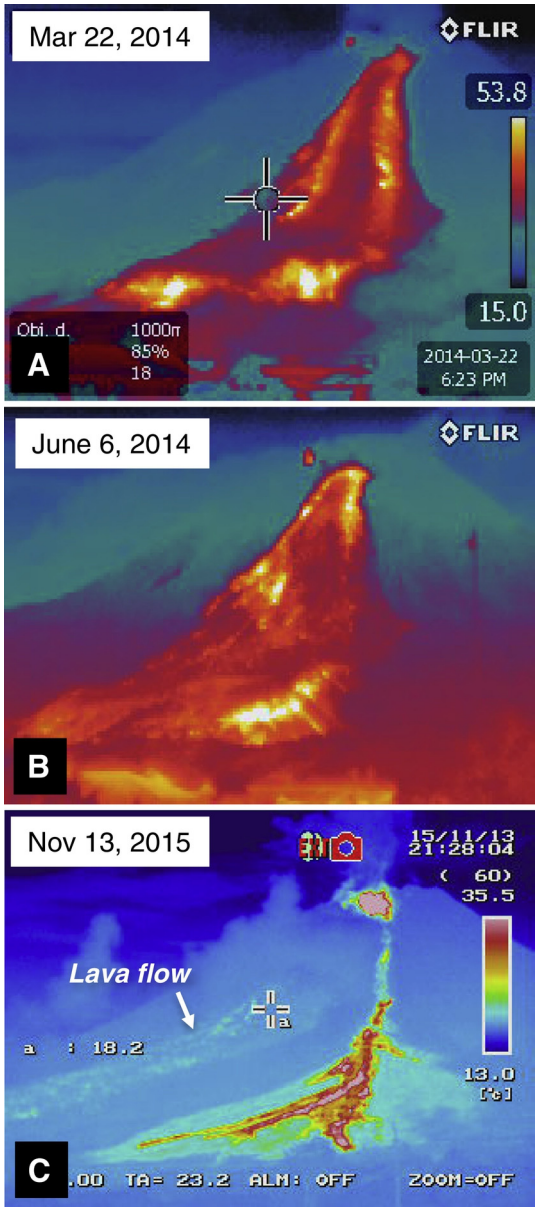

Fig. 8. Infrared camera images of the growing lava complex and the pyroclastic density current (PDC) deposits at Sinabung Volcano. A: Image of the lava complex taken from the Sinabung Volcano Observatory (POS) on the evening of March 22, 2014 (same as Fig. 6B). B: Image of the lava complex taken at POS on the evening of June 6, 2014. C: PDC deposit generated by lava collapse from the north side of the top of the lava complex (brightest part), with a seismic duration of about 3.5 min, on the morning of November 13, 2015, taken from the Bamboo site (6.5 km ENE of the summit) on the evening of the same day. Cooling lava complex ("lava flow") is seen extending from the center to the left of the photograph.

As partial collapses repeated in the upper part of the lava complex by late 2015, the complex was eroded on both sides by cascading PDCs and rock falls. Therefore, the upper part became knife-edge-like as seen in Figs. 3F and 4A.

5. Pyroclastic density current (PDC) events

Transport directions of PDCs were largely controlled by the morphology of the growing lava complex. Their travel distance depended on the height where collapse initiated and the relative elevation difference, irrespective of eruption stage. The travel distance of relatively large PDCs was limited in many cases by the banks of the Lau Borus River, which had heights of up to 50 m and running from east to south about 4–5 km away from the summit (Fig. 2). In January and February 2014, PDCs occurred from the front and margins of the growing lava complex (Fig. 6A). On February 1, 2014, a PDC event originated in the upper part of the lava complex and PDCs cascaded to the southeast (Fig. 6E), resulting in 16 fatalities from the associated pyroclastic surge at Sukameriah about 3 km from the summit (Fig. 2). The restricted danger zone had been set at 5 km in this direction. Subsequently the period from March to September 2014 was relatively quiet in terms of PDC events, even after the lava front reached the mountain foot (Fig. 7B). PDCs started cascading to the south-southeast from October 2014 to April 2015 (Fig. 2), when lava lobes repeatedly appeared in the southwestern side of the upper part of the lava complex. After May 2015, PDCs began moving to the east as lava lobes started growing in the northeastern side of the upper part of the lava complex. Less-frequently, PDCs generated simultaneously in both sides of the lava complex, for example, on May 21, 2015 and October 31, 2015 (Fig. 6G). From late 2015 to early 2016, PDCs traveled mainly to the east, and the villages

Please cite this article as: Nakada, S., et al., Growth process of the lava dome/flow complex at Sinabung Volcano during 2013–2016, J. Volcanol. Geotherm. Res. (2018), http://dx.doi.org/10.1016/j.jvolgeores.2017.06.012

of Simacem and Bekerah were buried by PDC deposits (Figs. 2 and 8C). On May 21, 2016, PDCs traveled about 5 km to the southeast and their surges reached a residential area across the Lau Borus River. Seven fatalities were reported in this farmland, although the area was within the danger zone (Fig. 6H).

When the January 11, 2014 PDCs reached the Lau Borus River, the POS observers reported that secondary explosions occurred in the river. The PDC deposits were about 3 m thick on the river bed, when inspected in August 2014 (Fig. 9A). Lava boulders of up to 1 m were present in the deposits and the ash matrix in contact with the boulders was light reddish brown due to oxidation during deposition (Fig. 9B). Segregation pipes were preserved in the matrix of the upper half of the deposits. The April 2, 2015 PDCs also reached the river, and the ash cloud surmounted the 50 m-high cliffs, reaching vegetable fields across a village road ~300 m laterally from the river bank (Figs. 2 and 9 D). Our field inspection 8 days after the event revealed that the vegetable fields were covered by an ash-cloud surge deposit of up to 15 cm thick; that houses, trees, and some animals were burned or singed in

Fig. 9. Photographs showing pyroclastic density current (PDC) deposits at Sinabung Volcano. A: PDC deposits from the January 11, 2014 event taken at the Lau Borus River on August 13, 2014. B: Juvenile lava blocks whose heat oxidized the surrounding matrix. C: PDC deposits from the April 2, 2015 event in the Lau Borus River. A white arrow points to a small crater of the secondary explosion. Taken on April 10, 2015. D: Tomato field affected by the ash-cloud surge of the April 2, 2015 event, when the PDCs reached the Lau Borus River and climbed an approximately 50 m-high cliff. The left side was affected by the surge. Taken near Sibintun on April 10, 2015. E: Section shows deposits from the primary surge and secondary explosion of the April 2, 2015 event. On the top of the south cliff of the Lau Borus River near Sibintun. Taken on May 12, 2015. F and G: PDC deposits of the April 30, 2015 event near Sukameriah. Taken on May 12, 2015. H: Lava blocks found in the deposits of the October 16 event, which were associated with a vulcanian explosion. An angular lava block surrounded by the surfaces shows the bread-crust bomb structure. Taken along the river bed near Gember on November 13, 2015.

Please cite this article as: Nakada, S., et al., Growth process of the lava dome/flow complex at Sinabung Volcano during 2013–2016, J. Volcanol. Geotherm. Res. (2018), http://dx.doi.org/10.1016/j.jvolgeores.2017.06.012

the surge area; and that fire was underway in a nearby small forest. The deposits on the southern cliff of the Lau Borus River, about 50 m above the river bottom, were also inspected (Fig. 9E). The primary surge deposit in this deposit was overlain by grayish layer, a few cm thick, made of coarse sand and small lava fragments, the latter of which were derived from the secondary explosions. The thickness of the secondary explosion layer varied over short distances and reached about 20 cm at the top of the cliff. Probable source locations of the secondary explosions were marked by circular pits up to a few meters across on the flat surface of the PDC deposits along the river bed (Fig. 9C).

6. Cyclic vulcanian events

The first vulcanian explosions after the appearance of lava in December 2013 took place in August 2015 (Gunawan et al., this issue), when hybrid event peaked (Fig. 5B). The explosions were characterized by emissions of ash clouds directly from the summit crater, which reached a few km above the summit. These explosions were accompanied by loud explosion noises that continued for a few hundreds of seconds (Fig. 6F). No larger collapses preceded these events. Similar explosive events have continued to the time this manuscript was written (February 2017), happening every a few hours or less in late 2015, every half a day in early 2016, and nearly every day in mid-2016. Clouds of vulcanian events were light to dark gray, in contrast to reddish brown ash clouds from collapse-triggered PDCs. Ejection of juvenile ballistics was also observed and ballistics were deposited near the crater (<1 km), which was confirmed by nighttime views of these incandescent blocks. The ash column rarely reached 5 km and was normally <3 km above the crater, based on observation from POS. Simultaneously with some of the vulcanian events, partial collapses of lava lobes in the upper part of the lava complex occurred (Fig. 6F). Furthermore, several PDCs originated from fountain-column collapses of vulcanian events. For example, PDCs deposits from October 16, 2015 and May 21, 2016 that reached the Lau Borus River, near the Gember village, contain bread-crust bombs with angular outlines as shown in Fig. 9H. The porosity of these blocks is variable, reaching as much as 58% vesicle space at the margins. Bread-crust bombs were not observed in collapse-triggered PDC deposits before these cyclic vulcanian events started. This clearly implies that inflation (vesiculation) of the lava block continued after fragmentation and during the explosion, suggesting that these eruptions tapped slightly deeper, less-degassed magma (Wright et al., 2007).

7. Chemical compositions

7.1. Analytical method

Chemical compositions of lava and volcanic ash samples were determined and show temporal chemical changes during the eruption. As volcanic ash consists of particles of crystals and glass of various origin, its bulk composition does not directly represent the chemistry of the magma. However, taking into account differential sorting of particles during transport, we can still utilize the bulk compositions of volcanic ash samples to characterize temporal change of magma chemistry. We have to rely on ash compositions because our access to PDC deposits and the lava complex was limited due to safety. Whereas, volcanic ash could be collected at more distal sites that were at safe distances from the eruption hazards. Samples were analyzed by a Rigaku ZSX Primus II, X-ray fluorescence analyzer at the Earthquake Research Institute (ERI), University of Tokyo, following the method of Hokanishi et al. (2015). Average whole-rock chemical compositions of pumice and lava samples from different events are shown in Table 2, and the bulk chemical compositions of volcanic ash samples are shown in Fig. 10 and Appendix Table 1. Additionally, Fig. 11 shows backscatter images of the groundmass of lava and volcanic ash samples taken with a JXA-8800R electron probe microanalyzer at ERI.

7.2. Chemical composition of pumice, lava, and volcanic ash

Pumice fragments a few centimeters across coming from a vulcanian explosion on November 23, 2013 were collected from the playground of an elementary school in Sigarangaran, which is about 3 km northeast of the volcano. Lava fragments in PDC deposits were taken in August 2014, April 2015, May 2015, November 2015, and October 2016. Volcanic ash, including lapilli from the January 5, 2014 event was taken from solar panels at the Sukanalu observation station by CVGHM observers. Volcanic ash samples were also collected intermittently at the foot of the volcano, near POS, and in the city of Berastagi, by CVGHM observers and us. Phenocrysts of plagioclase, pyroxenes, and amphibole are commonly present in juvenile materials.

Pumice fragments from a vulcanian event on November 23, 2013 contain 58 wt% SiO_2, which is more SiO_2–rich than lavas extruded from the summit in 2014 (Fig. 10A). Lavas erupted in 2015 and 2016 are, furthermore, more SiO_2-rich (Table 2 and Appendix Table 1). As the sampling opportunities were very limited, we have no way to know precisely when the chemical composition changed from 57 to 60 wt% SiO_2. Rock fragments in PDC events on October 16, 2015 and May 21, 2016, associated with vulcanian events, have a chemical composition similar to those for lava fragments erupted just before vulcanian events (Table 2). The phenocryst contents in lavas of the present eruption range from 35% to 40% in volume. The composition of volcanic ash from 2015 and 2016 is more evolved than fresh lavas (Fig. 10A). We attribute this difference in SiO_2 to crystal depletion in ash deposits. Volcanic ash elutriated from PDCs is very fine gained (commonly <0.1 mm across), because heavy and large grains stay coupled to the PDC or settle out from the ash cloud before reaching the sampling sites.

Alkaline elements are easily leached by hydrothermal alteration, as represented by samples of spine lava (Appendix Table 1), in which hornblende phenocrysts were completely replaced by pseudomorphs. Deficiencies of alkali elements in volcanic ash and spine lavas are expressed by differences of their compositions from the chemical trend formed by fresh lava samples for a given SiO_2 content (Fig. 10B). The alkali element deficiency was largest in the spine lava and decreased roughly with time from August–September 2010 to February 2014. Volcanic ash in 2010 and September–October 2013 represents products of phreatic events. Alkali deficiency may also result from incorporation of altered rock and soils exposed on the ground surface. Volcanic ash of PDCs in the early stage of lava complex growth shows a strong deficiency in alkalis (Fig. 10B), suggesting contribution of old altered materials along the pathway of PDCs. We infer that involvement of such old materials by PDCs diminished by mid-2014 as mountain slopes were blanketed by newly erupted volcanic deposits.

Fig. 11 shows backscatter images of the groundmass of three representative juvenile samples. The crystallinity of the groundmass did not increase over time, contrasting to increases in samples from the Mount St. Helens 1980–1986 and Unzen lava dome eruptions (Cashman, 1992; Nakada and Motomura, 1999). Our preliminary analyses of the crystallinity of the Sinabung groundmass, suggests a slight decrease with time (Fig. 11). Lava samples used for the crystallinity calculation were collected from the deposits of relatively large PDCs, which are considered to have been generated by partial collapses of the upper part of the lava complex and from bombs of the October 16, 2015 vulcanian events, which were transported in the PDCs. Therefore, it is considered that crystallization during motion after exiting the vent was minimal for the samples used for our crystallinity calculation. The crystallinities seen in Fig. 11 may represent the state of lava just as it exited the vent. Therefore, it is likely that the extent of the decompression-induced crystallization in the upper conduit (e.g., Cashman, 1992)

Please cite this article as: Nakada, S., et al., Growth process of the lava dome/flow complex at Sinabung Volcano during 2013–2016, J. Volcanol. Geotherm. Res. (2018), http://dx.doi.org/10.1016/j.jvolgeores.2017.06.012

Table 2
Whole rock chemical compositions of lava samples of the 2013–2016 Sinabung eruption.

Date[a]	2013/11/23	s.d.	2014/1/5	2014/1/11	s.d.	2015/4/2	s.d.	2015/4/28	2015/10/16	s.d.	2016/5/21	s.d.
N of samples	5		1	6		3		1	6		4	
(wt% dry basis)												
SiO_2	58.97	0.25	58.16	57.66	0.33	60.11	0.31	60.28	60.27	0.25	60.43	0.11
TiO_2	0.70	0.01	0.74	0.79	0.02	0.67	0.03	0.68	0.69	0.01	0.67	0.01
Al_2O_3	17.87	0.07	18.22	18.11	0.10	17.56	0.27	17.61	17.40	0.12	17.47	0.07
FeO[b]	6.76	0.10	7.07	7.42	0.25	6.50	0.28	6.35	6.42	0.11	6.26	0.10
MnO	0.16	0.00	0.16	0.16	0.00	0.15	0.01	0.15	0.15	0.00	0.15	0.00
MgO	2.85	0.06	2.89	2.99	0.08	2.62	0.14	2.55	2.66	0.05	2.59	0.06
CaO	7.73	0.10	8.03	8.12	0.10	7.22	0.19	7.17	7.18	0.15	7.15	0.03
Na_2O	2.97	0.02	2.92	2.94	0.03	3.00	0.03	3.04	3.06	0.01	3.09	0.01
K_2O	1.86	0.02	1.69	1.67	0.03	2.04	0.04	2.05	2.04	0.04	2.07	0.01
P_2O_5	0.12	0.00	0.12	0.13	0.00	0.13	0.01	0.13	0.14	0.00	0.13	0.00
$Na_2O + K_2O$	4.83	0.04	4.61	4.62	0.05	5.04	0.07	5.09	5.10	0.05	5.15	0.02
(ppm)												
Sc	20	1	22	22	1	18	1	19	20	2	18	1
V	158	4	172	176	6	147	5	142	145	4	141	4
Cr	3	2	4	7	5	3	2	2	7	2	6	1
Co	14	1	15	15	1	14	1	13	13	1	12	1
Ni	2	1	2	2	3	2	1	1	21	12	1	1
Cu	21	6	14	20	5	15	5	15	15	2	14	2
Zn	64	4	57	59	2	62	2	60	59	2	59	1
Ga	16	0	16	16	0	16	0	17	16	0	16	0
Rb	69	1	63	60	1	75	1	75	74	2	76	1
Y	26	0	26	27	0	27	0	27	28	1	26	0
Sr	334	2	342	341	4	330	3	330	329	4	327	2
Zr	123	2	115	113	1	138	3	139	144	5	140	1
Ba	380	9	349	345	7	447	4	464	433	7	439	5
Pb	15	1	12	13	1	15	4	14	15	0	14	1
La	21	1	17	18	1	26	4	22	27	2	22	3
Ce	54	5	55	49	3	64	5	65	48	2	55	2
Th	8	1	7	5	2	6	5	6	7	1	9	2

2013/11/23: Pumice pebbles at Sigarangaran about 3 km northeast of the summit (SNB20131221).
2014/1/5: A lava pebble on a solar panel at Skanal seismic station, 2 km east of the summit (SNB2014011).
2014/1/11: Lava blocks in the PDC deposit along the Lau Borus River, near Berastepu, 4 km southeast of the summit (SNB20140607).
2015/4/2: Lava pebbles in surge deposit on the southern cliff of the Lau Borus River near Sibintun, about 5 km south of the summit (SNB20150410).
2015/4/28: A lava block in PDC deposit near Sukameriah, about 3.5 km south of the summit (SNB20150511).
2015/10/16: Lava block (vesiculated) in PDC deposit near Gember, about 4.5 km southeast of the summit (SNB20151114).
2016/5/21: Lava blocks (vesiculated) in PDC deposit at Gember, about 5 km southeast of the summit (SNB20161018).
[a] Dates of pyroclastic density current (PDC) events.
[b] Total iron as FeO.

hardly changed with time even when the discharge rate decreased at Sinabung Volcano.

8. Temporal change of eruption product volume

8.1. Total erupted volume estimation

We estimated a total volume of eruption products (lava complex plus pyroclastic deposits) of ~1.76×10^8 m^3 ($1.09 + 0.67$, Table 1) by the end of June 2015, which is smaller than the ~2.8×10^8 m^3 volume estimation for June 21, 2015 by Yulianto et al. (2016). We carefully checked the difference, and found an overestimation of pyroclastic deposits in Yulianto et al. (2016). Although the lava complex volumes are similar to each other (1.1×10^8 m^3 vs. 0.9×10^8 m^3), the pyroclastic deposit volumes, which are distributed more extensively than the lava complex, shows a large difference. It is likely that the thickness of pyroclastic deposits was overestimated in Yulianto et al. (2016). For example, the topographic ridge contacting the northeast margin of the lava complex is thinly covered by pyroclastic surge (Fig. 2) such that the road could be recognized from a distance even in 2016, whereas Yulianto et al. (2016) reported a deposit thickness of over tens of meters there (Fig. 11 of Yulianto et al., 2016). Shrubs had grown sparsely in the area of new pyroclastic deposits in early 2017 at the place where the original topographic divide was covered by pyroclastic deposits of <10 m thick in our estimation (Figs. 2 and 4B). This suggests regrowth of shrubs that survived under a thin layer of pyroclastic deposits. Sparse growth of shrubs was also observed at the place facing the middle of the frontal cliff of the lava complex (at the site shown as the topographic divide in Fig. 4B). The thickness of the pyroclastic deposits just in front of the lava complex was estimated to be <10–20 m in this study (Fig. 4B), whereas Yulianto et al. (2016) reported 26–50 m there. Although the reason of their overestimation is not clear, our pyroclastic deposit thicknesses could be confirmed at several places in the field.

8.2. Volume change of pyroclastic deposits

The lava complex moved onto the southeastern slope, overlying new pyroclastic or talus deposits along its path in 2014. It is considered that there was negligible deposition of pyroclastic materials on the upper slopes at >1600 m asl, due to the high slope angle and erosion by the PDCs. The thickness of deposits that were buried by the lava complex was assumed to be 10 m below 1600 m asl, similar to the thickness of pyroclastic deposits in front of the lava complex (Fig. 4B). Multiplying this thickness by the area of the lava complex below 1600 m asl yields the volume of these PDC deposits beneath the lava complex of 1.19×10^7 m^3. Combining these values, results in a new total of PDC deposits of 7.88 ($(6.69 + 1.19) \times 10^7$ m^3). The adjusted total volume of the lava complex is 9.70×10^7 m^3 ($(10.89–1.19) \times 10^7$ m^3) (Table 1).

In this paper, we assumed that the cumulative volume of pyroclastic deposits is proportional to the cumulative numbers of PDC events. PDC events were distinguished from rock falls by longer duration on a seismogram in POS. For example, PDCs reaching about 3 km from the crater were

Please cite this article as: Nakada, S., et al., Growth process of the lava dome/flow complex at Sinabung Volcano during 2013–2016, J. Volcanol. Geotherm. Res. (2018), http://dx.doi.org/10.1016/j.jvolgeores.2017.06.012

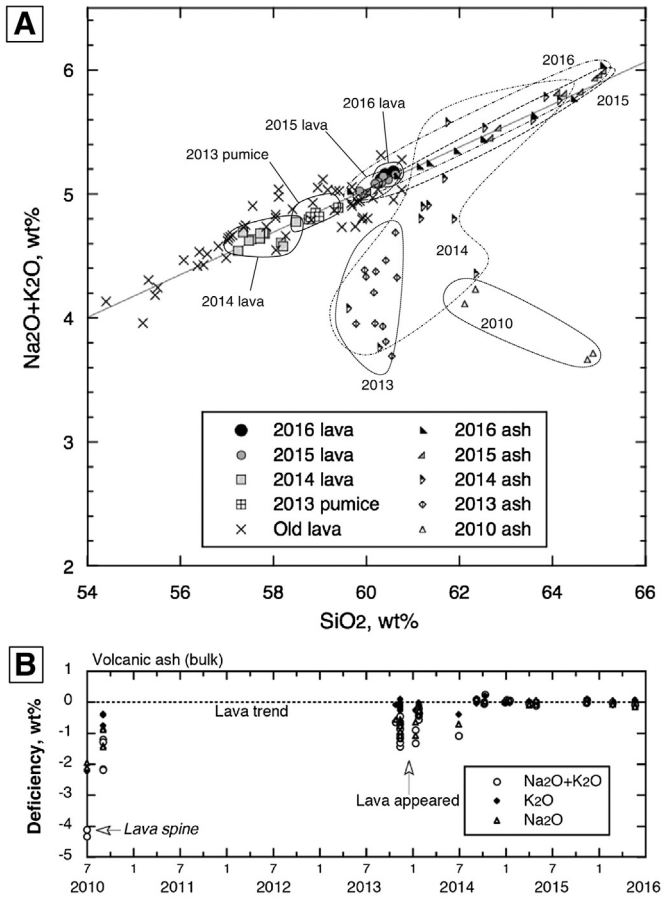

Fig. 10. A: Chemistry of whole rocks and bulk volcanic ash of Sinabung Volcano. B: Temporal change of alkali deficiency in volcanic ash. In A, "old lava" includes lavas from the 9th–10th century eruption. A straight line is the regression line for new lava samples ($[N_2O + K_2O] = 0.171 \times [SiO_2] - 5.25$). In B, deficiencies were expressed by differences in Na_2O, K_2O, and the total alkalis, respectively, to chemical trends formed by lavas from this eruption at a given SiO_2 content: [deficiency Na_2O] = $[Na_2O] - (0.0307 \times [SiO_2] - 1.18)$ and [deficiency of K_2O] = $[K_2O] - (0.144 \times [SiO_2] - 6.43)$. The leaching effect of K_2O during hydrothermal alteration is much smaller than that for Na_2O.

recorded as events with a seismic duration of 5 to 10 min in late February 2016. Four PDCs that reached the Lau Borus River (4.5 km) on May 21, 2016 had seismic durations as of > 14 min. There is a relationship between the volumes of the PDCs, their volumes, and duration of their seismic signals. However, large PDC events occurred rather randomly, and were always associated with a series of smaller PDC and rock fall events. Therefore, we used only the cumulative number of PDC events (Fig. 5C) to calculate the pyroclastic deposit volume through time. The detailed relationship between the PDC volumes and the seismic duration should be considered in the future by using individual seismic data for all events, such as was used in the volume estimation for the PDC deposits during the Unzen eruption by Takarada et al. (1993).

Thus, the real volume of PDC deposits is sensitive to estimates of the unit PDC deposit's volume, as it was calculated from the total volume of PDC deposits and the cumulative number of PDC events through June 25, 2015. The unit volume was estimated to be 39,300 m^3 (as 22,000 m^3 DRE). As approximately 2300 PDC events occurred as of the end of 2015, we estimated that the cumulative volume of pyroclastic deposits reached about 0.91×10^8 m^3 (0.57×10^8 m^3 DRE) by the end of 2015 (Table 1). We also calculate volume of deposits that were overlain by the lava complex during each period, using changing areas of the lava complex, and we subtracted these from the volume of the lava complex (Table 1). As we assumed a constant volume for all individual PDC events, the error is expected to be >20% of the results as shown in Fig. 12A.

8.3. Discharge rates

The lava volumes measured are consistent with volume estimates using DSM data for the end of June 2015 (Table 1). Our field observation indicated that the lava complex had hardly changed in volume and shape since the end of 2014, except in the upper part (Fig. 3E and F). However, the volume of the upper part of the lava complex is a minor part of the lava complex's total volume. It is clear that the total volume increased rapidly in the earliest stage and the rate of the increase later decreased (Fig. 12A); a relationship also documented by Pallister et al. (this issue). We calculated discharge rate based on the total volumes for the adjacent two periods (Fig. 12B). The discharge rate was highest in the initial stage and then decreased exponentially over time. This tendency is very close to estimates from GPS measurements (Fig. 5A; Hotta et al., this issue). The growth rate of a new lava lobe estimated in April 2015 (~0.7 m^3/s), described before, is also concordant with this trend. The discharge rate had been <0.5 m^3/s since the summer of 2015.

In the above volume estimation, we did not consider the volume of products from cyclic vulcanian events. According to the summary on vulcanian explosions at Sakurajima volcano during April–December 2008 (Tajima et al., 2013), the average column height of those explosions was approximately 1500 m and the average tephra mass was approximately 11,000 t (4400 m^3 DRE). The average column height of vulcanian events at Sinabung Volcano during November 2015–January 2017 was 1300 m, which is a little smaller than that at Sakurajima. The average daily number of vulcanian events at Sinabung was 2.3, according to observation data by CVGHM. On the other hand, the daily number of PDC events at Sinabung for the same period was 1.1. Assuming the eruption volumes of vulcanian

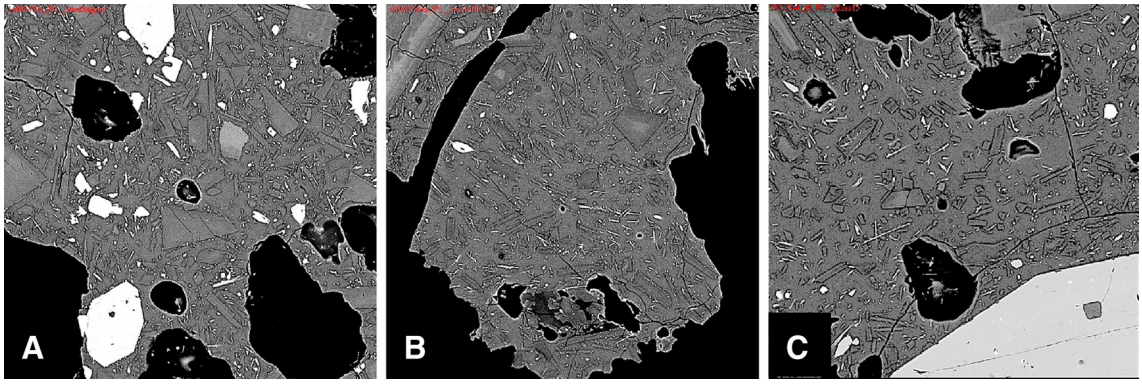

Fig. 11. Backscatter images showing groundmass texture of representative lava fragments at Sinabung Volcano. A: A juvenile pebble in volcanic ash from the January 5, 2014 pyroclastic density current (PDC) event, taken at Skanal observation site (SNB20140111-1). B: A juvenile particle in volcanic ash from early October 2014 PDC events, taken at the Skanal station (SNB20141007sknl_P2). C: A lava block from the October 16, 2015 PDC event, taken near Gember (SNB20151113-4). The groundmass crystallinity decreases from 39 vol% in A to 32 vol% in C. All widths of images are about 200 μm.

Please cite this article as: Nakada, S., et al., Growth process of the lava dome/flow complex at Sinabung Volcano during 2013–2016, J. Volcanol. Geotherm. Res. (2018), http://dx.doi.org/10.1016/j.jvolgeores.2017.06.012

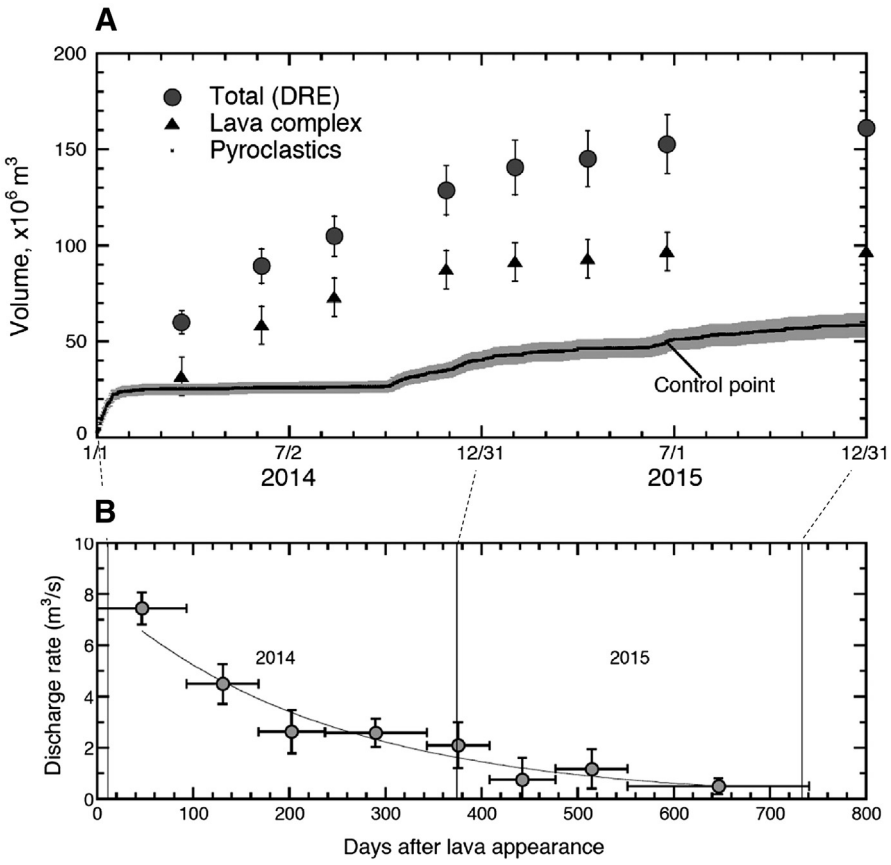

Fig. 12. A: Temporal volume change of the lava complex, pyroclastic deposits in dense-rock equivalent (DRE), and the total eruptive volumes at Sinabung Volcano. B: Temporal change in the discharge rate. The volumes of the lava complex were determined using a laser distance meter except for June and July 2015. The daily volumes of pyroclastic deposits were calculated using on the number of pyroclastic density current (PDC) events and average PDC unit volume based on digital surface model (DSM) data for June and July 2015 (see text). The total is the sum of the lava complex volumes and calculated volumes for pyroclastic deposits when the distance meter measurement was carried out. Volumes for the end of 2015 were estimated based on cumulative of PDC events as of that time, assuming a constant lava complex volume. The discharge rate was calculated for two adjacent measuring periods on the lava complex.

and PDC events as 4400 m^3 DRE and 22,000 m^3 DRE respectively (their daily numbers as 2.3 and 1.1 respectively), the daily volume of erupted products during the above period can be estimated as 34,300 m^3 DRE (10,100 + 24,200), which is equal to the discharge rate of 0.40 m^3/s. This implies that the discharge rate at Sinabung has been little changed since the vulcanian stage started.

9. Discussions

9.1. Mode of lava complex growth

Gunawan et al. (this issue) divided the eruption period into four phases: (i) first dome and collapse phase (December 18, 2013–January 10, 2014), (ii) lava flow phase (January 10, 2014–mid-September 2014), (iii) second lava dome and collapse phase (mid-September 2014–July 2015), and (iv) lava dome collapse and ash explosion phase (after August 2015). In this paper, the activity was divided into three stages mainly based on the fashion of the lava complex growth: (a) lava extension stage from late December 2013 to September 2014, (b) lava inflation stage from September 2014 to August 2015, and (c) vulcanian stage from August 2015. Although the vulcanian stage is the same as phase (iv) of Gunawan et al. (this issue), the first dome and collapse phase (i) and lava flow phase (ii) were both treated in the lava extension stage of this paper. The height of the lava complex above the crater increased over time (Fig. 7D) during the lava extension and inflation stages even after the movement of the lava's flow front became stagnated. This means the lava complex grew vertically from mid-2014 to mid-2015, and it is expected that the lava complex shape hardly changed as a whole in the vulcanian stage.

Apparent viscosity of flowing lava can be calculated from the advance speed of the lava complex, which can be introduced from the data in Fig. 7C. When the width of a flow is much larger than the thickness, $\eta = \rho g \sin\alpha\, h^2/3v_s$ (Harris and Rowland, 2015). Here, α is the slope angle (33° for the distance of the first 1 km, 15° for 1–2 km, and 9° for the last 0.5 km), h is the thickness of the lava flow (50, 80, and 100 m), v_s is the speed of the lava flow (60 m/day, 20 m/day, and 2 m/day), ρ is the density of a lava (2500 kg/m^3), g is the acceleration of gravity. Calculated viscosities were 1.6×10^{10} Pa s on the upper slope and 5.8×10^{11} Pa s on the lowest slope. Assuming Bingham flow, viscosity values become a little smaller than the above values: $\eta = (\rho g \sin\alpha\, h^2/v_s)\,((1 - h_p)/h)^2$ (e.g., Harris and Rowland, 2015) where h_p is the thickness of a plug flow. However, this depends on the assumed plug thickness.

The advance speed used above is not the actual speed of the lava flow, because advance is additionally controlled by the extent of rock failure at the moving front. Furthermore, the flow spread laterally near the lower flank of the volcano, so that the width of lava flow was neither constant nor much larger than its thickness on middle and higher slopes. Therefore, the above viscosity values on the middle and lower slopes are still higher than the real values. We consider that the viscosity of lava in the early stage at Sinabung was ~10^{10} Pa s or less. According to the scaling analysis on lava flows by Castruccio et al. (2013), the lava growth manner of the lava complex at Sinabung is similar to the lava flows at Colima, Mexico, in the volume-time term, and to Santiaguito, Guatemala, in the distance-time term. As both were considered examples controlled by "core yield strength" (Castruccio et al., 2013), the Sinabung lava complex might have flowed with a core yield strength of ~10^5 Pa and an apparent viscosity of ~10^9 Pa s as suggested by those examples.

Please cite this article as: Nakada, S., et al., Growth process of the lava dome/flow complex at Sinabung Volcano during 2013–2016, J. Volcanol. Geotherm. Res. (2018), http://dx.doi.org/10.1016/j.jvolgeores.2017.06.012

The apparent viscosity of the growing andesite lava dome at Soufrière Hills volcano was estimated to be about 10^{11} Pa s (Watts et al., 2002). That of a growing lava dome at Unzen ranges from 3×10^{10} to 4×10^{10} Pa s in the early stage of the eruption (Suto et al., 1993). The Unzen lava dome, which was growing on a slope as steep as that at Sinabung, did not reach more than about 1 km from the vent, contrasting to the lava flow at Sinabung which flowed up to about 3 km. Lavas were hornblende biotite dacite with 25–30 vol% phenocryst and a temperature of about 850 °C at Unzen (Nakada and Motomura, 1999) and hornblende pyroxene andesite of about 35 vol% phenocryst with a temperature ~950 °C at Sinabung (manuscript in preparation). Because of a higher magmatic temperature and more mafic composition of the lava, the lava of Sinabung may have been more fluid, meaning that it could flow in a longer distance.

9.2. Characteristics of Sinabung, compared with other dome eruptions

The Sinabung type of lava dome/flow eruption is similar in certain aspects to other historic eruptions such as at Unzen and Soufrière Hills volcanoes (Nakada et al., 1999; Watts et al., 2002). In those volcanoes, phreatic events preceded the appearance of lava at the summit crater and lava effusion was relatively continuous. Endogenous growth was observed at Mount St. Helens during the latter part of the 1980–1986 episode and at Unzen, when inflation of the oxidized broken part was followed by the formation of new small lava lobes repeatedly (Fink et al., 1990; Nakada et al., 1999). In both volcanoes, endogenous growth began when the discharge rate declined. At Unzen, endogenous growth was observed when discharge rates were <1.5 m^3/s. At Sinabung, endogenous growth was not clearly evident, even when the discharge rate decreased to <1 m^3/s. However, the movement of the lava front stagnated at the mountain foot around the summer of 2014, hybrid events increased in September 2014 (Fig. 5B), and inflation of the whole of the upper part of the lava complex occurred, such as increasing the maximum elevation and width of the upper part (Figs. 6B, C, and 7D). Measurement results by CVGHM using an Electric-Distance Meter (EDM) showed outward movement of the volcano eastern slope during the same period. This inflation may be considered as a sort of endogenous growth at Sinabung. The magma discharge rate during this stage had been around 2 m^3/s or lower (Fig. 12B).

The eruptive volume of the lava dome eruptions increased nearly exponentially with time as summarized in Fig. 13. It may be possible that overpressure of the magma chamber would not have approached to zero until 2016. The manner of the temporal discharge rate is close to what was modeled, for example, by Stasiuk et al. (1993) and Anderson and Segall (2011). At Sinabung, the discharge rate decreased monotonously with the increase in cumulative eruption volume (Fig. 14A). Stasiuk et al. (1993) showed that the relationship of the discharge rate and volume (Q* vs. V*, normalized to the initial rate and the final volume, respectively) can be used for testing the process of lava dome eruptions. This relationship for Sinabung is linear as seen in Fig. 14A, and similar to the model in which the discharge rate decreases as the magma chamber empties and the changes of conduit diameter and magma viscosity are minor during the eruption (Stasiuk et al., 1993). However, the discharge rate is inversely correlated with the height of the dome top at Sinabung as shown in Fig. 14B. The relationship for a model in which lava successively piles over the vent is different from the linear relationship between Q* and V* in Stasiuk et al. (1993). The geophysical model by Anderson and Segall (2011), which considers upper conduit physics and lava piling over the vent, seems to be able to explain the temporal

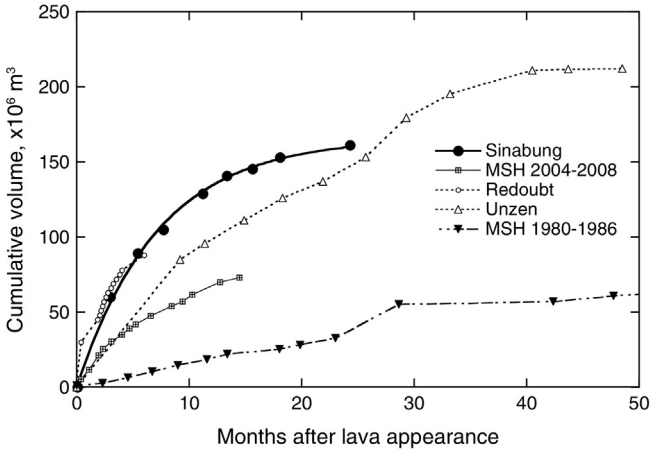

Fig. 13. Comparison of lava dome growth eruptions. The cumulative volumes of lava during the first 50 months are shown. The bold fitting line for Sinabung is the exponential growth line. Data, except Sinabung (this study) and Mount St. Helens of 1980–1986 are from Nakada et al. (1999). Data for Mount St. Helens 2004–2006 are from Mastin et al. (2008).

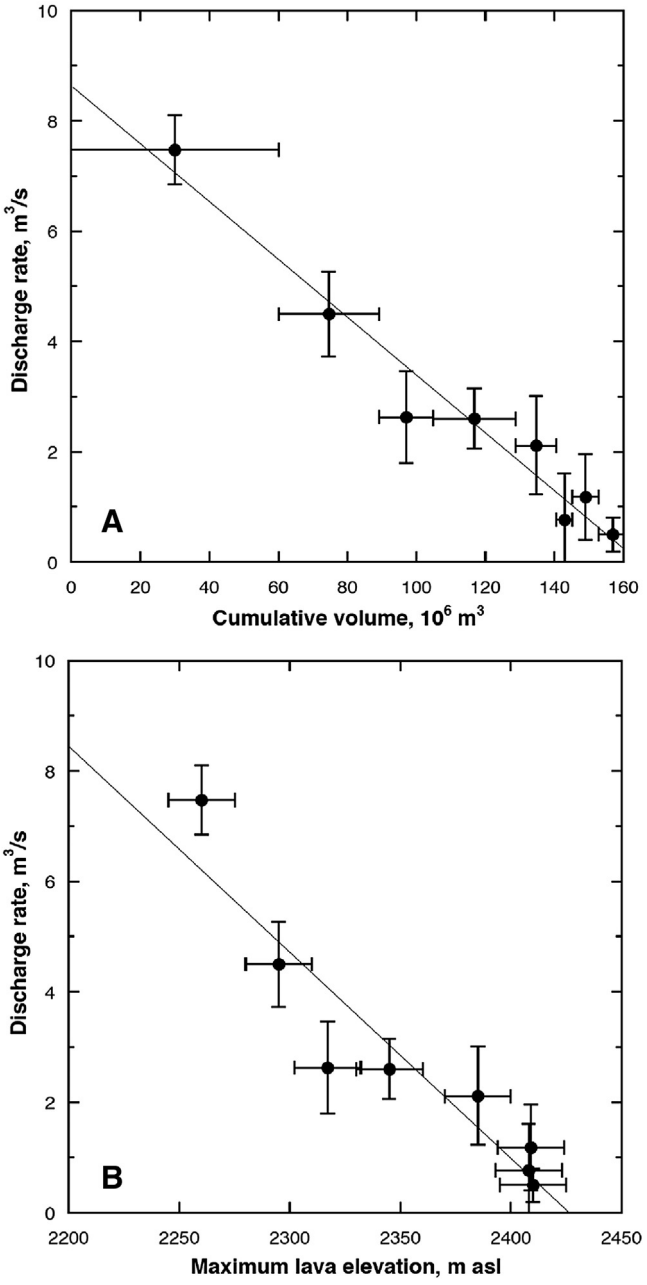

Fig. 14. Diagrams showing the discharge rate vs. the cumulative volume (A) and the maximum elevation of the lava dome complex (B) for Sinabung Volcano.

Please cite this article as: Nakada, S., et al., Growth process of the lava dome/flow complex at Sinabung Volcano during 2013–2016, J. Volcanol. Geotherm. Res. (2018), http://dx.doi.org/10.1016/j.jvolgeores.2017.06.012

changes among eruption volume, discharge rate, and dome top elevation in the Sinabung eruption.

9.3. The mechanism of cyclic vulcanian events

The vulcanian stage, which has continued since August 2015, is more complex than the above simple model. Globally, lava dome eruptions tend to end with the formation of a lava spine (e.g., Williams, 1932; Swanson et al., 1987; Nakada et al., 1999; Watts et al., 2002). Although explosive events did not occur just before the spine formation in these eruptions, repeated vulcanian events only occurred after large failures of lava domes on June 8 and 11, 1991 at Unzen (Nakada et al., 1999), and in August to October 1997 and in July 2003 at Soufrière Hills (Druitt et al., 2002; Herd et al., 2005). Magma ascent speeds during the formation of lava spines were summarized as $<1–5 \times 10^{-4}$ m/s by Cashman et al. (2008). Assuming a diameter of 30 m for the upper conduit, this speed is equal to the discharge rate of <0.07–0.35 m^3/s which is close to the discharge rate during the vulcanian stage of Sinabung. The superficial explosion of the growing dome is also possible due to the development of an impermeable carapace, which builds up the inner pressure of growing dome (Boudon et al., 2015). Boudon et al. (2015) suggested that the likelihood of superficial dome explosions depends inversely on lava dome volume. That is, a large lava dome does not keep an impermeable carapace due to its increasing thickness and the development of deep cracks. The vulcanian stage of Sinabung began after its lava complex became large, thus it cannot be explained by this model.

Products of the vulcanian events at Unzen and Soufrière Hills are highly vesiculated, showing polygonal shape with breadcrust surfaces (Nakada et al., 1999; Druitt et al., 2002). Rock fragments found in PDC deposits of the vulcanian stage at Sinabung are also vesiculated (up to 58% of porosity), which are similar to products at Soufrière Hills (55%–75% of porosity) (Druitt et al., 2002), and contrast with the massive lava fragments in PDC deposits from before the vulcanian stage at Sinabung. Druitt et al. (2002) suggested that the explosions at Soufrière Hills were derived from brittle fragmentation of overpressured magma in the upper conduit prior to each event. The discharge rate during the explosions at Sourfière Hills was estimated to have increased with time, ranging from 3 to 10 m^3/s (Calder et al., 2002), much higher than during the vulcanian stage at Sinabung.

Another example of cyclic explosions has been documented at the Santiaguito dacite dome (Bluth and Rose, 2004), where strombolian to small vulcanian explosions have continued for a long time. Explosions there repeated every ten minutes at discharge rates lower than 1 m^3/s. Holland et al. (2011) proposed a model in which explosions were caused by repeated healing of fractured marginal solidifying lava in the upper conduit, which was networked with many cracks that were utilized for degassing. They estimated that the time scale for healing of fractured lava is close to the eruption hiatus for explosions. It is unlikely that this model is directly applicable directly to Sinabung, because the time intervals of explosions is much shorter at Santiaguito than at Sinabung, and because the magma is hotter and more mafic at Sinabung.

We suggest that eruptive behavior during the vulcanian stage at Sinabung indicates that the magma's degassing became restricted, contrasting with effective degassing in the earlier stages. Cashman et al. (2008) summarized that a low ascent speed allows for extensive decompression crystallization in the upper conduit and the formation of a plug of solidifying magma, which can become a lava spline. However, the groundmass crystallinity of the lava at Sinabung seems to have been nearly constant or slightly decreased slightly over time (Fig. 11). This supports the idea that degassing became somewhat more restricted in the later stage at Sinabung, as an increase in decompression crystallization is not observed. Also, deformation and seismic data, discharge rate, and magma chemistry hardly changed just before and during the vulcanian stage (Figs. 5A and 12B, Table 2). These observations do not favor replenishment of new volatile-rich magma during the vulcanian stage. Nearly constant or decreasing crystallinity of the lava suggests that the rate of decompression-induced crystallization hardly changed in the upper conduit, even as the discharge rate decreased. Such conditions could be achieved using a model similar to Holland et al. (2011). In such a model, conduit walls, which were initially highly fractured and allowed effective degassing, were then coated on the inside by solidification of new ascending lava, in addition to annealing of the fractured marginal lava. Therefore, the effective diameter of the upper conduit became small, keeping the magma ascent speed unchanged, and thus explosive events occurred due to less degassing than before.

When the load of a lava dome becomes balanced with the overpressure of the magma chamber, lava dome eruption should stop. At the end of the eruptions, dacite lava thickened about 240 m over the vent at Unzen and 260–250 m at Mount St. Helens for the 1980–1986 and 2004–2006 eruptions (Nakada et al., 1999; Swanson and Holcomb, 1990; Mastin et al., 2008). In contrast, it is common for vulcanian events to occur soon after the formation of relatively thin andesite lava domes in craters; for example, Asama in 2004 (Urabe et al., 2006) and Kirishima in 2011 (Maeno et al., 2013), where lava thicknesses before the onset of explosive events were 60 and 120 m, respectively. At Sinabung, the thickness of andesite lava covering the vent is ~150 m (Fig. 14B), where the steep slopes prevented lava piling over the vent effectively. It is likely that the load of lava above the vent was not enough to balance the overpressure of the magma chamber after the summer of 2015 at Sinabung. A steady magma discharge at low rate under an incomplete degassing system in the upper conduit had caused cyclic vulcanian events for more than a year and half.

10. Concluding remarks

Lava dome/flow eruption at Sinabung began at the end of 2013 continued for >3 years. The initial magma discharge rate of >7 m^3/s decreased exponentially over time. The lava complex extended to the foot of the volcano through steep upper and middle slopes, repeating partial collapses and decreased its advance speed over time (lava extension stage). When the lava front movement became stagnated before a runout of ~3 km from the crater, the lava complex, especially in the upper part, started inflating at a discharge rate of ~2 m^3/s or less (lava inflation stage). New lava lobes appeared repeatedly on both sides of the upper part of the lava complex starting in late 2014. These lobes disappeared one after another due to repeating partial collapses and due to their instability on steep upper slopes. Cyclic vulcanian events began in August 2015, and continued >1.5 years (vulcanian stage). Vulcanian explosions repeated a few times a day when the discharge rate was <0.5 m^3/s.

PDC events occurred frequently during the growth of the lava complex and were less frequent when the lava complex front approached the volcano foot. Even at a discharge rate of <0.5 m^3/s, PDCs traveled about 5 km from the crater as collapses initiated at the highest points. Cyclic vulcanian events sometimes triggered partial collapses of the lava complex at its upper part near the vent.

Lava of this eruption was andesite and chemically evolved roughly with time as much as ~3 wt% in SiO_2. Due to steepness of the upper slopes at Sinabung, the lava over the vent did not thicken. Thus, the load of the lava may not have been balanced with overpressure of the magma chamber. In addition, as degassing of the magma within the upper conduit became restricted, explosive events may have continued even after the discharge rate became <0.5 m^3/s.

Acknowledgments

Field survey and volcanic ash sampling were largely helped by Armen Putra. This research was carried by a part of JST/JICA SATREPS "Integrated study on mitigation of multimodal disasters caused by ejection of volcanic products", and supported partly by JSPS KAKENHI Grant Numbers 25350493 and 16K01313. The DSM analysis in this study was supported by T. Chiba. Comments on early manuscript by Heather Wright and Fidel Costa were very helpful to complete this paper.

Please cite this article as: Nakada, S., et al., Growth process of the lava dome/flow complex at Sinabung Volcano during 2013–2016, J. Volcanol. Geotherm. Res. (2018), http://dx.doi.org/10.1016/j.jvolgeores.2017.06.012

Appendix A

Appendix Table 1
Bulk compositions of volcanic ash samples of the 2010–2016 eruption and lava spine samples at Sinabung Volcano.

Sample name	Remarks	SiO_2	TiO_2	Al_2O_3	FeO[a]	MnO	MgO	CaO	Na_2O	K_2O	P_2O_5	$Na_2O + K_2O$	Sc	V	Cr	Co	Ni	Cu	Zn	Ga	Rb	Y	Sr	Zr	Ba	Pb	La	Ce	Th
SNB11031002	Lava spine	76.30	0.85	6.94	7.21	0.16	2.78	1.97	1.58	2.14	0.07	3.71	11	141	9	15	1	11	68	13	85	17	96	169	495	10	7	28	11
SNB11031004	Lava spine	75.95	0.91	6.60	7.60	0.16	3.01	2.26	1.41	2.03	0.06	3.43	14	188	4	17	1	4	69	10	91	23	79	180	501	14	14	44	12
SNB AB-1	Aug/Sep. 2010	64.87	0.83	18.34	5.87	0.08	1.82	4.31	1.77	1.94	0.17	3.72	16	156	7	13	3	24	82	18	84	25	361	146	459	39	27	63	7
SNB AB-2	Aug/Sep. 2010	64.75	0.84	18.47	5.93	0.08	1.80	4.30	1.73	1.93	0.17	3.67	16	157	4	12	3	23	74	18	84	24	359	144	444	40	30	56	7
SNB AB-3	Aug/Sep. 2010	62.34	0.82	17.43	6.61	0.13	2.69	5.57	2.27	1.96	0.17	4.23	17	158	5	13	2	49	94	18	79	26	339	139	410	42	25	51	6
SNB Jaka-L	Aug/Sep. 2010	62.11	0.79	17.76	6.85	0.11	2.34	5.76	2.21	1.90	0.16	4.11	18	158	3	13	0	46	88	17	75	26	341	138	426	38	27	48	9
SNB131025	Oct. 2013	60.41	0.73	17.19	6.82	0.14	3.12	6.96	2.47	1.99	0.15	4.46	20	154	7	13	3	44	107	16	68	28	331	133	373	44	22	66	4
SNB131101	Nov. 2013	60.62	0.74	17.27	6.55	0.14	3.39	6.43	2.49	2.20	0.18	4.69	19	152	5	14	2	29	114	17	78	29	325	147	423	57	29	64	6
SNB131103	Nov. 2013	60.66	0.72	17.18	6.82	0.13	2.99	7.02	2.32	2.01	0.17	4.33	19	152	4	14	2	44	100	17	76	28	346	144	427	52	23	67	8
SNB131108	Nov. 2013	60.20	0.72	17.34	6.80	0.14	3.09	7.18	2.35	2.02	0.16	4.37	20	156	2	13	2	35	92	17	74	27	342	141	423	51	24	62	8
SNB131110-1	Nov. 2013	59.96	0.73	17.57	6.91	0.15	3.03	7.10	2.45	1.94	0.15	4.39	18	154	3	13	1	24	89	17	66	26	332	131	380	45	24	53	4
SNB131110-2	Nov. 2013	60.00	0.71	17.62	6.84	0.13	2.77	7.45	2.37	1.96	0.16	4.33	18	146	11	12	2	18	76	16	67	26	326	133	401	46	25	56	6
SNB131111	Nov. 2013	59.77	0.74	17.63	7.36	0.12	2.91	7.35	2.10	1.86	0.16	3.95	19	158	1	14	0	18	80	16	64	28	336	135	406	57	20	59	5
SNB131114-1	Nov. 2013	60.55	0.74	17.72	7.13	0.11	2.61	7.29	1.87	1.83	0.16	3.69	21	160	7	14	3	23	73	17	68	27	331	136	416	61	27	63	9
SNB131114-2	Nov. 2013	60.42	0.73	17.71	6.98	0.12	2.72	7.35	1.97	1.84	0.15	3.81	20	161	5	13	2	19	72	16	67	27	334	133	404	57	24	62	7
SNB131118-1	Nov. 2013	60.16	0.73	17.68	6.87	0.12	2.81	7.26	2.28	1.93	0.16	4.21	18	153	3	15	2	23	82	16	73	28	347	139	406	48	27	65	9
SNB131118-2	Nov. 2013	60.19	0.74	17.65	6.97	0.12	2.76	7.46	2.09	1.87	0.16	3.96	19	159	3	13	2	23	78	17	68	28	345	137	414	51	21	61	7
SNB131118-3	Nov. 2013	60.35	0.74	17.79	6.97	0.11	2.62	7.33	2.09	1.84	0.16	3.93	19	157	6	14	2	24	78	16	68	26	340	137	411	54	21	61	7
SNB140111-1	Jan. 2014	59.63	0.78	18.30	7.38	0.12	2.37	7.20	2.38	1.70	0.14	4.08	19	175	6	14	4	20	56	16	60	25	344	116	375	19	22	50	7
SNB140111-2	Jan. 2014	60.29	0.64	19.34	7.58	0.07	1.52	6.63	1.97	1.80	0.17	3.76	19	156	5	14	5	26	56	17	63	23	377	124	412	20	25	59	7
SNB140123-2	Jan. 2014	61.89	0.66	18.22	5.85	0.11	2.08	6.24	2.67	2.13	0.14	4.80	16	132	5	12	4	31	60	17	78	28	328	142	445	42	24	64	9
SNB140123-4	Jan. 2014	61.69	0.62	18.76	5.78	0.12	1.97	5.78	2.89	2.24	0.15	5.13	15	125	6	10	6	27	53	17	82	28	325	149	465	29	22	68	10
SNB140123-5	Jan. 2014	61.23	0.63	18.39	6.29	0.11	1.93	6.39	2.82	2.07	0.14	4.90	16	142	6	11	6	31	54	16	75	26	331	134	447	31	26	54	9
SNB140123-6	Jan. 2014	61.17	0.63	18.45	6.37	0.11	1.91	6.41	2.75	2.05	0.14	4.80	17	141	4	11	6	33	57	16	74	26	337	136	429	30	28	56	8
SNB140124-2	Jan. 2014	61.34	0.64	18.49	6.36	0.11	1.85	6.15	2.80	2.11	0.14	4.91	16	140	3	12	6	34	73	16	74	25	336	135	439	25	25	56	9
SNB140629 SKNL	Jun. 2014	62.36	0.72	17.50	6.43	0.10	2.02	6.38	2.40	1.95	0.13	4.36	18	150	5	10	2	21	56	16	72	24	337	139	427	30	21	63	10
SNB140907 POS	Sep. 2014	63.87	0.48	17.89	4.22	0.11	1.70	5.81	3.26	2.52	0.14	5.78	15	79	3	9	3	19	52	16	93	28	302	166	502	34	24	78	12
SNB141006 BRSTG	Oct. 2014	62.56	0.67	17.03	5.92	0.13	2.13	5.90	3.12	2.42	0.13	5.54	16	128	2	11	4	17	89	16	89	28	297	170	504	24	26	74	8
SNB141007 BRSTG	Oct. 2014	63.59	0.61	17.31	5.15	0.12	1.92	5.58	3.11	2.49	0.13	5.60	15	110	3	10	2	18	352	19	91	28	297	184	542	28	34	82	9
SNB141007 SKNL	Oct. 2014	64.16	0.54	17.59	4.52	0.11	1.71	5.49	3.18	2.57	0.14	5.76	14	95	4	9	1	17	50	16	94	28	302	185	574	26	29	83	12
SNB141010 POS	Oct. 2014	61.76	0.58	17.22	6.80	0.12	1.87	5.90	3.12	2.46	0.16	5.58	15	108	13	13	6	19	71	17	87	27	309	170	531	34	27	72	10
SNB141227	Dec. 2014	64.61	0.48	17.59	4.27	0.10	1.60	5.40	3.19	2.63	0.13	5.82	14	89	1	7	3	14	46	15	96	29	301	185	557	22	32	86	10
SNB150104	Jan. 2015	64.11	0.50	17.31	4.52	0.11	1.66	5.84	3.22	2.59	0.12	5.82	13	100	5	7	2	17	46	15	94	28	300	171	531	20	29	74	9
SNB150110	Jan. 2015	64.27	0.49	17.33	4.35	0.11	1.74	5.78	3.21	2.60	0.12	5.81	15	88	1	8	3	14	45	15	95	29	294	178	538	20	28	77	10
SNB150116	Jan. 2015	64.93	0.49	16.94	4.38	0.11	1.64	5.45	3.25	2.68	0.12	5.94	14	89	0	8	2	17	64	15	94	29	285	182	568	22	26	81	10
SNB2015041002	Apr. 2015	59.94	0.63	17.85	6.32	0.15	2.54	7.44	2.98	2.02	0.12	5.00	19	144	5	14	2	13	60	17	74	27	331	136	430	15	26	66	6
20150512-01	May 2015	62.68	0.61	17.55	5.18	0.13	2.04	6.23	3.11	2.34	0.13	5.45	16	114	0	11	3	17	57	17	89	28	313	161	516	18	25	71	10
SNB151114 LKW	Nov. 2015	65.05	0.56	16.87	4.05	0.10	1.60	5.65	3.33	2.65	0.14	5.98	15	80	5	7	2	17	42	15	101	30	292	184	526	20	28	55	11
SNB151114 SGRGR	Nov. 2015	65.17	0.57	16.81	4.15	0.10	1.56	5.49	3.32	2.69	0.14	6.00	16	82	3	9	2	18	44	15	102	30	291	186	556	20	34	56	11
SNB151113-8	Nov. 2015	60.05	0.73	17.48	6.63	0.15	2.72	7.10	3.02	2.00	0.14	5.02	21	148	6	13	11	13	61	16	73	27	328	140	410	15	26	49	7
SNB151114 MRDD	Nov. 2015	65.08	0.51	16.86	4.14	0.10	1.62	5.52	3.33	2.70	0.13	6.04	13	83	5	8	1	15	43	15	100	29	289	183	539	20	29	70	12
SNB160205 LKW	Feb. 2016	59.64	0.72	17.12	7.25	0.16	2.82	7.12	3.02	2.01	0.14	5.02	18	161	7	15	1	13	136	17	74	26	320	137	426	17	23	56	10

Values in wt% for major oxides (dry basis) and in ppm for minor elements.
Remarks: Months and years of eruption events except for top two samples from old lava spine at the summit.
[a] Total iron as FeO.

References

Anderson, K., Segall, P., 2011. Physics-based models of ground deformation and extrusion rate at effusively erupting volcanoes. J. Geophys. Res. 116:B7204. http://dx.doi.org/10.1029/2010JB007939.

Bluth, G.J.S., Rose, W.I., 2004. Observations of eruptive activity at Santiaguito volcano, Guatemala. J. Volcanol. Geotherm. Res. 136, 297–302.

Boudon, G., Balcone-Bissard, H., Villemant, B., Morgan, D.J., 2015. What factors control superficial lava dome explosivity? Sci. Rep. 5:14551. http://dx.doi.org/10.1038/srep14551.

Calder, E.S., Luchett, R., Sparks, R.S.J., Voight, B., 2002. Mechanism of lava dome instability and generation of rockfalls and pyroclastic flows at Soufrière Hills Volcano, Montserrat. In: Druitt, T.H., Kokellar, B.P. (Eds.), The Eruption of Soufrière Hills Volcano, Montserrat, from 1995 to 1999. Geol. Soc. London, Mem 21, pp. 173–190.

Cashman, K.V., 1992. Groundmass crystallization of Mount St. Helens dacite, 1980–1986: a tool for interpreting shallow magma processes. Contrib. Mineral. Petrol. 109: 431–449. http://dx.doi.org/10.1007/BF00306547.

Cashman, K.V., Thornber, R., Pallister, J.S., 2008. From dome to dust: shallow crystallization and fragmentation of conduit magma during the 2004–2006 dome extrusion of Mount St. Helens, Washington. A Volcano Rekindled: The Renewed Eruption of Mount St. Helens, 2004–2006. U.S. Geol. Surv., Prof. Pap 1750, pp. 387–413.

Castruccio, A., Rust, A.C., Sparks, R.S.J., 2013. Evolution of crust- and core-dominated lava flows using scaling analysis. Bull. Volcanol. 75:681. http://dx.doi.org/10.1007/s00445-012-0681-2.

Chesner, C.A., Rose, W.I., Deino, A., Drake, R., Westgate, J.A., 1991. Eruptive history of Earth's largest Quaternary caldera (Toba, Indonesia) clarified. Geology 19, 200–203.

Druitt, T.H., Young, S.R., Baptie, B., Bonadonna, C., Calder, E.S., Clarke, A.B., Cole, P.D., Harford, C.L., Heard, R.A., Luchett, R., Ryan, G., Voight, B., 2002. Episodes of cyclic vulcanian explosive activity with fountain collapse at Soufrière Hills Volcano, Montserrat. In: Druitt, T.H., Kokelaar, B.P. (Eds.), The Eruption of Soufrière Hills Volcano, Montserrat, from 1995–1999. Geol. Soc. London, Mem 21, pp. 281–306.

Fink, J.H., Malin, M.C., Anderson, S.W., 1990. Intrusive and extrusive growth of the Mount St. Helens lava dome. Nature 348, 435–437.

Global Volcanism Program, 2010. Report on Sinabung (Indonesia). In: Wunderman, R. (Ed.), Bulletin of the Global Volcanism Network, 35:7 Smithsonian Institution. http://dx.doi.org/10.5479/si.GVP.BGVN201007-261080.

Global Volcanism Program, 2013. Report on Sinabung (Indonesia). In: Wunderman, R. (Ed.), Bulletin of the Global Volcanism Network, 38:9 Smithsonian Institution. http://dx.doi.org/10.5479/si.GVP.BGVN201309-261080.

Global Volcanism Program, 2014a. Report on Sinabung (Indonesia). In: Wunderman, R. (Ed.), Bulletin of the Global Volcanism Network, 39:1 Smithsonian Institution. http://dx.doi.org/10.5479/si.GVP.BGVN201401-261080.

Global Volcanism Program, 2014b. Report on Sinabung (Indonesia). In: Wunderman, R. (Ed.), Bulletin of the Global Volcanism Network, 39:10 Smithsonian Institution. http://dx.doi.org/10.5479/si.GVP.BGVN201410-261080.

Gunawan, H., Surono, Budianto, A., Kristianto, Prambada, O., McCausland, W., Pallister, J., Iguchi, M. Overview of the eruptions of Sinabung eruption, 2010 and 2013-present and details of the 2013 phreatomagmatic phase. J. Volcanol. Geotherm. Res., this issue.

Harris, A.J.L., Rowland, S.K., 2015. Lava flows and rheology. In: Sigurdsson, H., et al. (Eds.), The Encyclopedia of Volcanoes, second edition Academy Press, pp. 321–342.

Herd, R.A., Edmonds, M., Bass, V.A., 2005. Catastrophic lava dome failure at Soufrière Hills Volcano, Montserrat, 12–13 July 2003. J. Volcanol. Geotherm. Res. 148:2340252. http://dx.doi.org/10.1016/j.jvolgeores_2005.05.003.

Hill, E.M., Borrero, J.C., Huang, Z., Qiu, Q., Banerjee, P., Natawidjaja, D., et al., 2012. The 2010 Mw 7.8 Mentawai earthquake: very shallow source of a rare tsunami earthquake determined from tsunami field survey and near-field GPS data. J. Geophys. Res. 117 (B06402). http://dx.doi.org/10.1029/2012JB009159.

Hokanishi, N., Yasuda, A., Nakada, S., 2015. Major and trace element analysis of silicate rocks using fused glass beads with an X-ray fluorescence spectrometer. Bull. Earthq. Res. Inst., Univ. Tokyo 90, 1–14 (in Japanese).

Holland, A.S.P., Watson, I.M., Phillips, J.C., Caricchi, L., Dalton, M.P., 2011. Degassing processes during lava dome growth: insites from Santiaguito lava dome, Guatermala. J. Volcanol. Geotherm. Res. 202:153–166. http://dx.doi.org/10.1016/j.jvolgeores.2011.02.004.

Hotta, K., Iguchi, M., Ohkura, T., Hendrasto, T., Gunawan, H., Rosadi, U., Kriswati, E. Process of magma intrusion and effusion at Sinabung volcano, Indonesia, during the eruptive activity from 2013a to 2016, as revealed from continuous GNSS observation data. J. Volcanol. Geotherm. Res., this issue.

Iguchi, M., Surono, Nishimura, T., Hendrasto, M., Rosadi, U., Ohkura, T., Triastuty, H., Basuki, A., Loeqman, A., Maryant, S., Ishinara, K., Yoshimoto, M., Nakada, S., Hokanishi, N., 2012. Methods for eruption prediction and hazard evaluation at Indonesian volcanoes. J. Disaster Res. 7, 26–36.

Kokelaar, B.P., 2002. Setting, chronology and consequences of the eruption of Soufrière Hills Volcano, Montserrat (1995–1999). In: Druitt, T.H., Kokelaar, B.P. (Eds.), The Eruption of Soufrière Hills Volcano, Montserrat, from 1995–1999. Geol. Soc. London, Mem 21, pp. 1–43.

Kozono, T., Ueda, H., Ozawa, T., Koyaguchi, T., Fujita, E., Tomiya, A., Suzuki, Y.J., 2013. Magma discharge variations during the 2011 eruptions of Shinmoe-dake volcano, Japan, revealed by geodetic and satellite observations. Bull. Volcanol. 75:695. http://dx.doi.org/10.1007/s00445-013-0695-4.

Maeno, F., Nakada, S., Nagai, M., Kozono, T., 2013. Ballistic ejecta and eruption condition of the vulcanian explosion of Shinmoedake volcano, Kyushu, Japan on February, 2011. Earth Planets Space 65:609–621. http://dx.doi.org/10.5047/eps.2013.03.004.

Mastin, L., Roeloffs, E., Beeler, N.M., Quick, J.E., 2008. Constraints on the size, overpressure, and volatile content of the Mount St. Helens magma system from geodetic and dome-growth measurements during the 2004–2006+ eruption. In: Sherrod, D.R., et al. (Eds.), A Volcano Rekindled: The Renewed Eruption of Mount St. Helens, 2004–2006. US, Geol. Surv., Prof. Pap 1750, pp. 461–488.

McCausland, W., White, R., Indrastuti, N., Gunawan, H., Patria, C., Suparman, Y., Putra, A., Tristuty, H., Hendrasto, M., 2017. Using a process-based model of pre-eruptive seismic patterns to forecast evolving eruptive styles at Sinabung Volcano, Indonesia. J. Volcanol. Geotherm. Res. http://dx.doi.org/10.1016/j.jvolgeores.2017.04.004 in press.

Melnik, O., Sparks, R.S.J., 1999. Nonlinear dynamics of lava dome extrusion. Nature 402, 37–41.

Nakada, S., Motomura, Y., 1999. Petrology of the 1991–1995 eruption at Unzen: effusion pulsation and groundmass crystallization. J. Volcanol. Geotherm. Res. 89, 173–196.

Nakada, S., Shimizu, H., Ohta, K., 1999. Overview of the 1990–1995 eruption at Unzen Volcano. J. Volcanol. Geotherm. Res. 89, 1–22.

Ogburn, S.E., Loughlin, S.C., Calder, E.S., 2015. The association of lava dome growth with major explosive activity (VEI ≥ 4): DomeHaz, a global dataset. Bull. Volcanol. 77 (40). http://dx.doi.org/10.1007/s00445-015-0919-x.

Pallister, J.S., Diefenbach, A.K., Burton, W.C., Muñoz, J., Griswold, J.P., Lara, L.E., Lowenstern, J.B., Valenzuela, C.E., 2013. The Chaitén rhyolite lava dome: eruption sequence, lava dome volumes, rapid effusion rates and source of the rhyolite magma. Andean Geol. 40:277–294. http://dx.doi.org/10.5027/andgeoV40n2-a06.

Pallister, J., Wessels, R., Griswold, J., Kartadinata, N., Gunawan, H., Budianto, A., Primulyana, S. 2017 Remote sensing of the Sinabung eruption: use of Optical, IR and Satellite Radar Imagery to monitor activity, estimate effusion rates, forecast collapse events and map the distribution of pyroclastic deposits. J. Volcanol. Geotherm. Res., this issue.

Prambada, O., Zaennuddin, A., Iryanto, Santosa, I., Nakada, S., Yoshimoto, M., 2011. Geologic map of Sinabung Volcano, North Sumatra Province (1:25.000). Center for Volcanology and Geological Hazard Mitigation. Geological Agency.

Stasiuk, M.V., Jaupart, C., Sparks, R.S.J., 1993. On the variations of flow rate in non-explosive lava eruptions. Earth Planet. Sci. Lett. 114, 505–516.

Sutawidjaja, I.S., Prambada, O., Siregar, D.A., 2013. The August 2010 phreatic eruption of Mount Sinabung, North Sumatra. Indian J. Geol. 8, 55–61.

Suto, S., Sakaguchi, K., Watanabe, K., Saito, E., Kawanabe, Y., Kazahaya, K., Takarada, S., Soya, T., 1993. Dynamics of flowage and viscosity of the 1991 1ava of Unzen volcano, Kyushu, Japan. Bull. Geol. Surv. Jpn 44, 609–629 (in Japanese).

Swanson, D.A., Holcomb, R.T., 1990. Regularities in growth of the Mount St. Helens dacite dome, 1980–1986. In: Fink, J.H. (Ed.), Lava Flows and Domes. Emplacement Mechanisms and Hazard Implications. Springer-Verlag, New York, pp. 3–24.

Swanson, D.A., Dzurisin, D., Holcomb, R.T., Iwatsubo, E.Y., Cadwick Jr., W.W., Casadevall, T.J., Ewert, J.W., Heliker, C.C., 1987. Growth of the lava dome at Mount St. Helens, Washington, (USA), 1981–1983. U.S. Geol. Surv. Spec. Pap. 212, 1–27.

Tajima, Y., Tamura, K., Yamakoshi, T., Tsune, A., Tsurumoto, S., 2013. Ellipse-approximated isopach maps for estimating ashfall volume at Sakurajima Volcano. Bull. Volc. Soc. Japan 58, 291–306.

Takarada, S., Kazahaya, K., Kawanabe, Y., Sakaguchi, K., Suto, S., Yamamoto, M., Soya, T., Unzen Weather Station, 1993. Volume estimation of 1991–1992 eruption of Unzen Volcano, and initiation mechanisms of pyroclastic flows on June 3 and June 8, 1991. Bull. Geol. Surv. Jpn 44, 11–24 (in Japanese).

Urabe, B., Watanabe, N., Murakami, M., 2006. Topographic change of the sumit crater of Asama Volcano during the 2004 eruption derived from airborne synthetic aperture radar (SAR) measurements. Bull. Geospat. Inform. Auth. Japan (GSI) 53, 1–6.

Watts, R.B., Herd, R.A., Sparks, R.S.J., Young, S.R., 2002. Growth patterns and emplacement of andesitic lava dome at Soufrière Hills Volcano, Montserrat. In: Druitt, T.H., Kokelaar, B.P. (Eds.), The Eruption of Soufrière Hills Volcano, Montserrat, from 1995–1999. Geol. Soc. London, Mem 21, pp. 11–152.

Williams, H., 1932. The history and character of volcanic domes. Bull. Dep. Geol. Sci., Univ. California 21, 51–146.

Wright, H.M., Cashman, K.V., Rosi, M., Cioni, R., 2007. Breadcrust bombs as indicators of Vulcanian eruption dynamics at Guagua Pichincha volcano, Ecuador. Bull. Volcanol. 69:281. http://dx.doi.org/10.1007/s00445-006-0073-6.

Yulianto, F., Suwarsono, Sofan, P., 2016. The utilization of remotely sensed data to analyze the estimated volume of pyroclastic deposits and morphological changes caused by the 2010–2015 eruption of Sinabung Volcano, North Sumatra, Indonesia. Pure Appl. Geophys. 173:2711–2725. http://dx.doi.org/10.1007/s00024-016-1342-8.

Please cite this article as: Nakada, S., et al., Growth process of the lava dome/flow complex at Sinabung Volcano during 2013–2016, J. Volcanol. Geotherm. Res. (2018), http://dx.doi.org/10.1016/j.jvolgeores.2017.06.012